frontiers | Frontiers in Marine Science

TYPE Original Research
PUBLISHED 23 September 2024
DOI 10.3389/fmars.2024.1469283

OPEN ACCESS

EDITED BY
Fei Li,
Southwest Petroleum University, China

REVIEWED BY
Zhang Yi,
Chongqing University, China
Chunhua Shi,
Guizhou University, China

*CORRESPONDENCE
Ping Wang
wangping_2016@163.com

RECEIVED 23 July 2024
ACCEPTED 30 August 2024
PUBLISHED 23 September 2024

CITATION
Wang P, Wang J, Du Y, Yu W, Zhou Q, Tian L, Yuan L, Pan W, Wei W, Qin Y and Ma Z (2024) Manganese mineralization constrained by redox conditions in the Cryogenian Nanhua Basin, South China and its implications for nitrogen and carbon cycling. *Front. Mar. Sci.* 11:1469283. doi: 10.3389/fmars.2024.1469283

Manganese mineralization constrained by redox conditions in the Cryogenian Nanhua Basin, South China and its implications for nitrogen and carbon cycling

Ping Wang[1]*, Jian Wang[1], Yuansheng Du[2], Wenchao Yu[2], Qi Zhou[3], Li Tian[4], Liangjun Yuan[5], Wen Pan[5], Wei Wei[2], Yongjun Qin[3] and Zhixin Ma[3,6]

[1]School of Resources and Environment, Henan Polytechnic University, Jiaozuo, China, [2]School of Earth Sciences, China University of Geosciences, Wuhan, China, [3]Engineering Technology Innovation Center of Mineral Resources Explorations in Bedrock Zones, Ministry of Natural Resources, Guiyang, China, [4]State Key Laboratory of Marine Environmental Science, Xiamen University, Xiamen, China, [5]103 Geological Party, Guizhou Bureau of Geology and Mineral Exploration and Development, Tongren, China, [6]Chengdu Center, China Geological Survey, Chengdu, China

The Nanhua Basin of South China recorded complete Cryogenian stratigraphic sequence from the Sturtian Glaciation (~717–660 Ma) to the Marinoan Glaciation (~654–635 Ma). The interglacial Datangpo Fm in the Nanhua Basin is divided into two members, and the first member consists of the Mn-carbonate unit and the overlying black shale unit, containing a series of large and superlarge manganese deposits. The metallogenic process of manganese deposits is not clear, and the Mn-carbonates formed through the precursor of Mn-oxide/oxyhydroxide reduction or directly precipitated from an anoxic water column. Moreover, the redox conditions in the deep Nanhua Basin during the precipitation of manganese deposits are also controversial. In this study, the high-resolution nitrogen contents (TN), isotope compositions, carbon isotope compositions of organic and inorganic matter from the first member of the Datangpo Fm are analyzed. The $\delta^{15}N$ values of the Mn-carbonate unit (+1.53‰ to +5.26‰, mean +3.36‰) are higher than those of the overlying black shale unit (−3.74‰ to +3.54‰, mean +0.89‰). The Mn contents show a negative relationship with TN but a positive relationship with $\delta^{15}N$ in the Mn-carbonate unit, implying that the formation of Mn-carbonates is related to redox variations. The relatively higher $\delta^{15}N$ values in the Mn-carbonate unit indicated oxic conditions, and NH_4^+can be released and partially oxidized during the mineralization of organic matter, resulting in the residual ^{15}N-enriched NH_4^+ being transferred into clay minerals. Meanwhile, the lower $\delta^{15}N$ values in the black shale unit indicated anoxic conditions, which recorded primary N isotope signals. The Mn-carbonate unit is characterized by negative $\delta^{13}C_{carb}$ values (−11.17‰ to −5.22‰, mean −8.30‰), which show a positive relationship with $\delta^{13}C_{org}$, but a negative relationship with Mn contents, implying that the negative $\delta^{13}C_{carb}$ excursions were related to the organic matter degradation during Mn-carbonate formation. The findings of this study indicated that the metallogenesis of manganese deposits in the Cryogenian Nanhua Basin was constrained mainly by the oxic interval in the deep basin. The nitrogen and carbon cycling process can provide new insights into geochemical cycling after the Sturtian Glaciation.

KEYWORDS

Mn-carbonate, black shale, nitrogen isotope, carbon isotope, negative carbon isotope excursions, metallogenesis

1 Introduction

The Earth experienced two global glaciation events in the Neoproterozoic Era (~1,000–542 Ma), i.e., the older Sturtian Glaciation (~717–660 Ma) and the younger Marinoan Glaciation (~654–635 Ma) (Kirschvink, 1992; Hoffman et al., 1998; Hoffman and Schrag, 2002). Sedimentary manganese deposits precipitated widely during this period in Brazil, Namibia, India, and South China (Roy, 2006; Yu et al., 2016). Mn was preserved as Mn-carbonates in India and South China (Roy et al., 1990; Gutzmer and Beukes, 1998; Yu et al., 2016; Zhou et al., 2016), but as Mn-oxides interbedded with banded iron formations (BIFs) in Namibia and Brazil (Bühn et al., 1992; Klein and Ladeira, 2004; Cabral et al., 2011). A series of large–superlarge manganese deposits were discovered in the post-Sturtian deep Nanhua Basin of South China (Zhou et al., 2016, 2022).

It is generally considered that the metallogenic processes of the manganese deposits in the Cryogenian Nanhua Basin of South China experienced two stages (Yu et al., 2016, 2017; Wu et al., 2016; Xiao et al., 2017). During Stage I, the dissolved Mn^{2+} sourced mainly from hydrothermal activity (Wu et al., 2016; Yu et al., 2016) were oxidized to Mn-oxides/oxyhydroxides under oxic conditions and then sank to organic matter-enriched sediments. During Stage II, the insoluble Mn-oxides/oxyhydroxides were reduced to Mn^{2+} in porewater during the organic matter mineralization, which subsequently reacted with HCO_3^- and were preserved as Mn-carbonates during the sedimentary-early diagenetic process ($2MnO_2 + CH_2O + HCO_3^- \rightarrow 2MnCO_3 + H_2O + OH^-$). The organic matter acted as electron acceptor during the reduction of Mn-oxides/oxyhydroxides and can be oxidized to ^{13}C-depleted HCO_3^-. Both stages were mediated by microbial activities (Roy, 2006; Yu et al., 2016, 2019). The oxidation of dissolved Mn^{2+} was mediated by enzymatic multicopper oxidase processes associated with autotrophic microbial activity under oxic conditions (Tebo et al., 2004; Morgan, 2005; Yu et al., 2019), whereas the Mn-oxide/oxyhydroxide reduction to Mn^{2+} in porewater was mediated by heterotrophic microbes under suboxic conditions (Yu et al., 2019), similar to the Jurassic Úrkút manganese deposits in Hungary (Polgári et al., 2012a, 2012b). However, an alternative metallogenic process of the manganese deposits was recently proposed, during which the Mn-carbonates were directly precipitated from the anoxic water column in the Cryogenian Nanhua Basin (Ai et al., 2023).

The redox conditions of the post-Sturtian Nanhua Basin are still controversial. Some studies suggested that the deep Nanhua Basin was anoxic, after which the oxygenation expanded (e.g., Cheng et al., 2021; Wu et al., 2024). However, other studies have shown that the deep Nanhua Basin experienced episodic ventilation, similar to the Baltic Sea (Yu et al., 2016; Xiao et al., 2017; Ai et al., 2021). Furthermore, the relationship between redox conditions and the metallogenic process of sedimentary manganese deposits in the Cryogenian Nanhua Basin still needs to be further studied. The negative carbon isotope excursions of the Mn-carbonate unit of the manganese deposits in the Cryogenian Nanhua Basin were reported, ranging between −5‰ and −12‰ (mean ca. −8‰) (e.g., Li et al., 1999; Zhou et al., 2007; Chen et al., 2008; Wu et al., 2016; Qu et al., 2018; Zhu et al., 2019; Pei et al., 2020; Tan et al., 2021). The negative $\delta^{13}C_{carb}$ excursions might be related to organic matter, which can provide ^{13}C-depleted carbon (Li et al., 1999; Chen et al., 2008; Wu et al., 2016; Qu et al., 2018; Zhu et al., 2019; Dong et al., 2023). However, how the ^{13}C-depleted organic matter affected the carbon isotope compositions of the Mn-bearing sediments and whether the negative $\delta^{13}C_{carb}$ excursions are related to the formation of Mn-carbonates remain unclear.

This study focuses on the drillcore ZK2115, which is located in the Gaodi Manganese Deposit, eastern Guizhou Province. The high-resolution nitrogen and carbon geochemical data are analyzed for the Mn-carbonate unit and the overlying black shale unit of the post-Sturtian Datangpo Fm. Combined with the previously reported total organic carbon (TOC) and Mn contents in the study units, the redox proxy-$\delta^{15}N$ values suggested that the deep basin was oxic during the precipitation of the Mn-carbonate unit, which facilitated the metallogenic process of the manganese deposits. The Mn-carbonate formation experienced the Mn^{2+} oxidation and reduction stages, leading to the negative $\delta^{13}C_{carb}$ excursions in the basal Datangpo Fm. Carbon and nitrogen cycling in the Cryogenian is reconstructed, which can also provide new insights for the global N–C cycling throughout Earth's history.

2 Geological background

The Nanhua Basin developed as a rift basin between the Yangtze Block and Cathaysia Block during the breakup of the Rodinia supercontinent in Neoproterozoic (Dalziel, 1991; Hoffman, 1991; Moores, 1991; Li et al., 2008; Wang and Pan, 2009) (Figures 1A, B). The Nanhua Rift Basin consists of Wuling and Xuefeng secondary rift basins and the Tianzhu–Huitong Uplift between them. The Wuling Secondary Rift Basin consists of a series of NE–SE-trending grabens and horsts (Zhou et al., 2016, 2022), and a series of manganese deposits precipitated in the small grabens of the rift basin in a similar spreading direction (Figure 1C).

The Nanhua Basin recorded complete Cryogenian stratigraphic sequence, including the Tiesi'ao Fm, Datangpo Fm, and Nantuo Fm (Figure 2A). The Tiesi'ao and Nantuo formations recorded glaciomarine sediments during the Sturtian and Marinaon glaciations, while the Datangpo Fm recorded the interglacial sediments between the two global glaciations. The Datangpo Fm is subdivided into two members, the first member consists of the Mn-carbonate unit and the overlying black shale unit, while the second member consists of gray siltstones. The manganese deposits discovered in the Cryogenian Nanhua Basin are called "Datangpo-type" manganese deposits. Moreover, the coeval cap carbonates precipitated in the horsts of the Nanhua Basin (Yu et al., 2017, 2020). There are two types of manganese ores in the "Datangpo-type" manganese deposits, i.e., banded ores (Figure 2B) and massive ores (Figure 2C). In the "Datangpo-type" manganese deposits, the thickness of the Mn-carbonate unit decreased from the center of the basin to the edge, whereas the ore types changed from massive ores to banded ores, accompanied by the decreasing Mn contents (Zhou et al., 2013, 2022). The study drillcore ZK2115 is located in the Gaodi Manganese Deposit (Figure 1C).

The termination of the Sturtian Glaciation was globally synchronous and limited to ca. 660 Ma through zircon U-Pb and Re-Os dating (e.g., Rooney et al., 2015; Hoffman et al., 2017). The similar radiometric ages were also reported in South China. For example, the uppermost Tiesi'ao Fm yielded a Re-Os age of 660.6 ± 3.9 Ma (Rooney et al., 2020). The Mn-carbonate unit of the Datangpo Fm yielded zircon U-Pb ages of ca. 660 Ma through LA-ICP-MS (Yu et al., 2017; Ma et al., 2023), SIMS (Wang et al., 2019a), ID-TIMS (Zhou et al., 2004), CA-ID-TIMS (Rooney et al., 2020; Zhou et al., 2020), and SHRIMP (Yin et al., 2006), with a Re-Os age of 660.6 ± 7.5 Ma (Pei et al., 2017). Moreover, the coeval post-Sturtian cap carbonates in South China also yielded a similar zircon U-Pb age of 658.8 ± 0.5 Ma via CA-ID-TIMS (Zhou et al., 2019). The geochronological lines of evidence can also be used to constrain the formation age of the "Datangpo-type" manganese deposits.

3 Samples and methods

The present study focuses on the drillcore ZK2115 (Figure 1). A total of 38 samples were collected from the first member of the Datangpo Fm, including 24 samples from the Mn-carbonate unit (~11 m) and 14 samples from the black shale unit (~30 m).

The collected fresh samples avoiding veins were cleaned and crushed to ~200 mesh before geochemical analyses. The TN contents, inorganic carbon and oxygen isotope, and organic carbon isotope compositions were conducted at the State Key Laboratory of Geological Processes and Mineral Resources, China University of Geosciences (Wuhan).

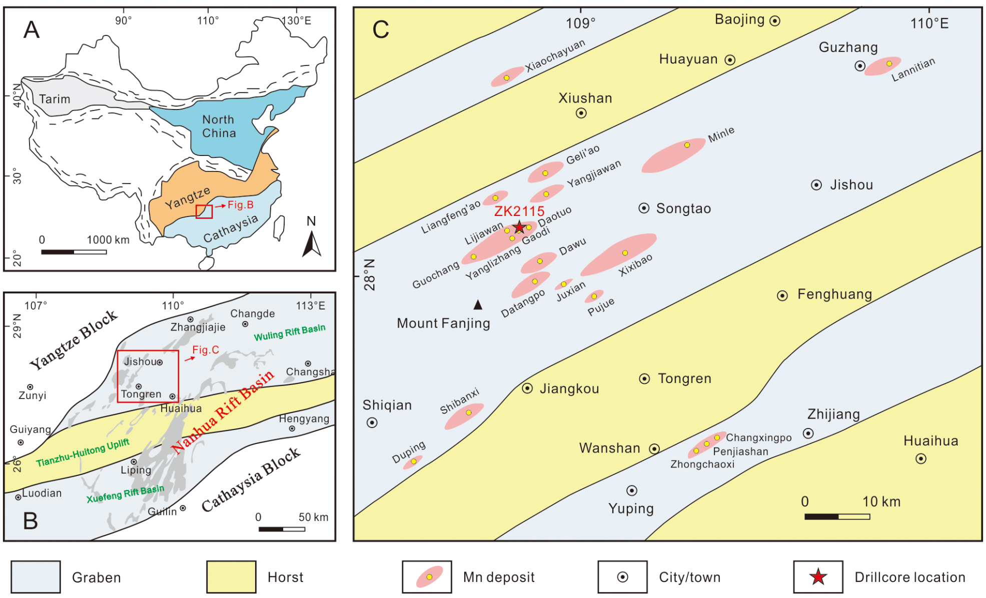

FIGURE 1
(A) Tectonic units of China. **(B)** Structure of the Nanhua Rift Basin on the southeast margin of the Yangtze Block (Zhou et al., 2016). **(C)** Distribution of Datangpo-type manganese deposits in the Guizhou–Hunan–Chongqing adjacent area (modified from Zhou et al., 2016, 2022). The study drillcore ZK2115 is marked by red stars.

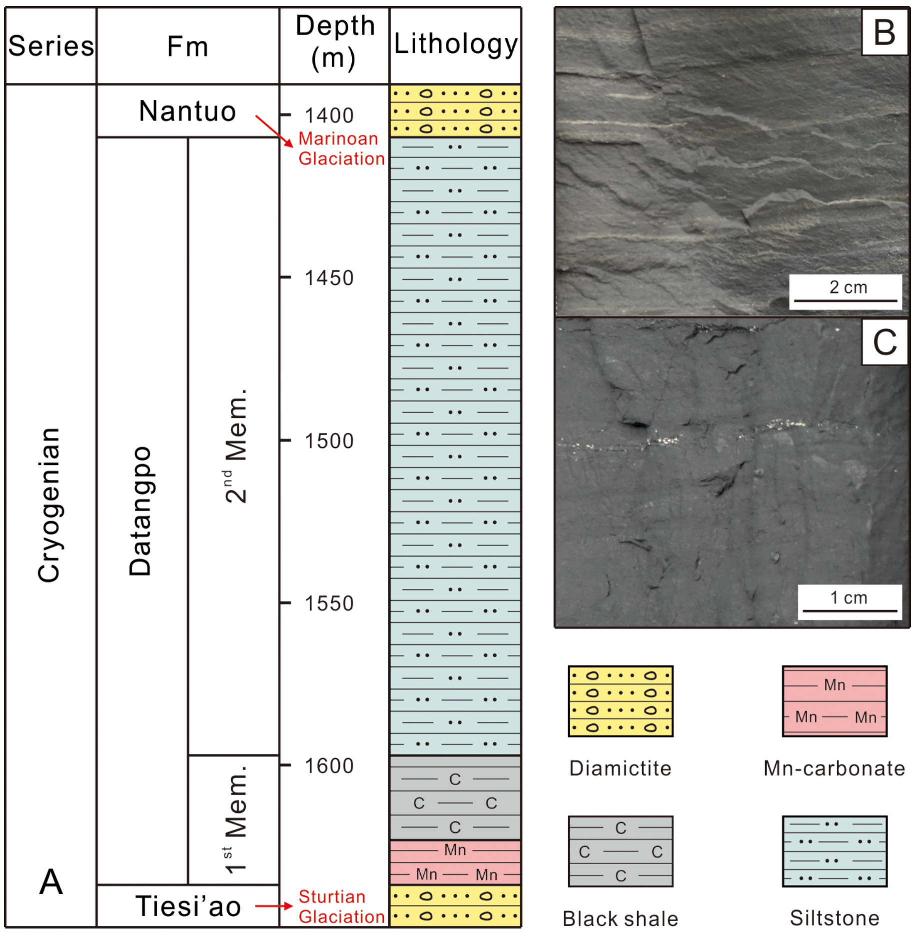

FIGURE 2
(A) Cryogenian stratigraphic sequence of drillcore ZK2115 in the Nanhua Basin of South China. Two ore types of the "Datangpo-type" manganese deposits precipitated in the basal Datangpo Fm, i.e., banded ores **(B)** and massive ores **(C)**.

The TN contents were analyzed in an Elementar Vario MACRO CUBE element analyzer, and the analytical precisions are better than 0.02%. The inorganic carbon and oxygen isotope compositions were analyzed using a MAT253 isotope ratio mass spectrometer. The results are expressed in delta notation as per mil (‰) deviations relative to Vienna Pee Dee Belemnite (VPDB) standard ($\delta^{13}C = [(^{13}C/^{12}C)_{sample}/(^{13}C/^{12}C)_{VPDB} - 1] * 1{,}000$). The analytical precisions are better than 0.1‰ based on two laboratory standards (GBW04416 and GBW04417).

Before the nitrogen and organic carbon isotope analyses, the carbonate portions should be removed. The powder samples were treated with 4 M hydrochloric acid until the carbonates were completely reacted. Then, the residues were rinsed by deionized water for several times until pH tests gave a near-neutral value (≥6.0). The samples were then centrifuged and dried in the oven at 50°C. The carbonate-free samples were analyzed using an EA +MAT253 isotope ratio mass spectrometer. The results are also expressed in delta notation as per mil (‰) deviations relative to the VPDB standard ($\delta^{13}C = [(^{13}C/^{12}C)_{sample}/(^{13}C/^{12}C)_{VPDB} - 1] * 1{,}000$). The analytical precisions are better than 0.06‰, and the analysis results are based on three laboratory standards (GBW04407, GBW04408, and ACET).

The carbonate-free $\delta^{15}N$ values of the study samples were analyzed in EA+IRMS (isotope ratio mass spectrometry; IsoPrime 100) at the State Key Laboratory of Marine Environmental Science, Xiamen University. The results are reported using standard delta notation as deviations ($\delta^{15}N = [(^{15}N/^{14}N)_{sample}/(^{15}N/^{14}N)_{standard} - 1] * 1{,}000$); the standard is atmospheric N_2 with a $\delta^{15}N$ value of 0‰. The analytical precisions are better than 0.1‰ based on laboratory standards (USGS40, GUGS41, and IAEA-600).

4 Results

All geochemical data for the Mn-carbonate unit and the black shale unit are given in Table 1. The TN contents range from 0.02% to 0.12% (mean 0.06%) in the Mn-carbonate unit and from 0.07% to 0.10% (mean 0.08%) in the black shale unit (Figure 3). The $\delta^{15}N$ values decrease from the Mn-carbonate unit (+1.53‰ to +5.26‰, mean +3.36‰) to the overlying black shale unit (−3.74‰ to

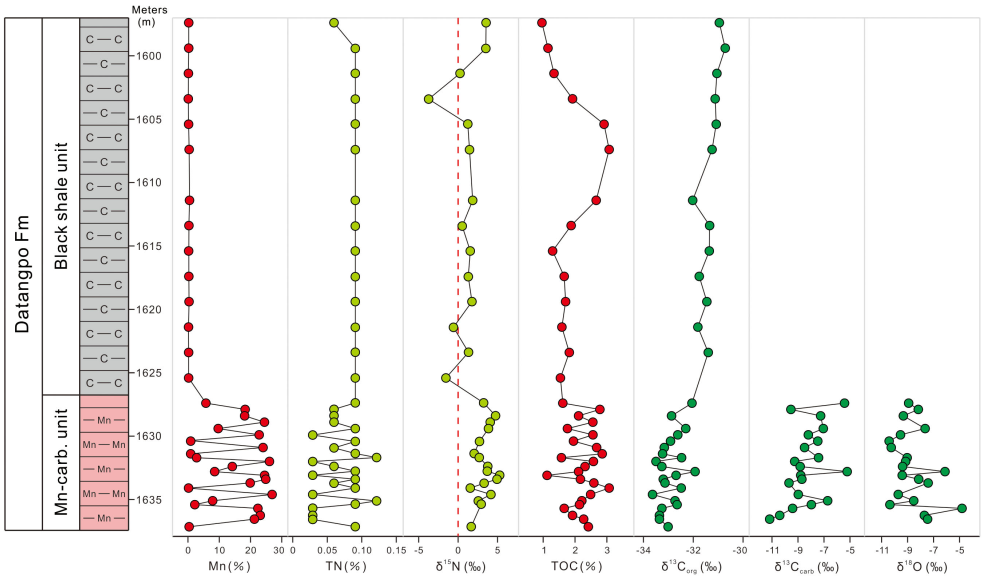

FIGURE 3
Geochemical profiles of drillcore ZK2115 for the first member of the Datangpo Fm, located in the Gaodi Deposit, Guizhou Province. TOC and Mn contents are collected from Wang et al. (2019b).

+3.54‰, mean +0.89‰) (Figure 3). The $\delta^{13}C_{org}$ values vary from −33.61‰ to −31.82‰ (mean −32.84‰) in the Mn-carbonate unit and from −31.92‰ to −30.55‰ (mean −31.20‰) in the black shale unit (Figure 3). Meanwhile, the $\delta^{13}C_{carb}$ values range between −11.17‰ and −5.22‰ (mean −8.30‰) in the Mn-carbonate unit, while the $\delta^{18}O$ values range between −10.14‰ and −4.81‰ (mean −8.57‰) (Figure 3). The C/N values range between 14.9 and 128.6 (mean 56.0) in the Mn-carbonate unit, which are higher than the black shale unit (15.8 to 44.2, mean 25.8).

5 Discussion

5.1 The nitrogen and carbon isotope evaluation of the post-Sturtian Datangpo Fm

The nitrogen isotope compositions of sedimentary rocks are used to reflect local redox conditions in the water column of ancient oceans and reconstruct biogeochemical N cycling (e.g., Sigman et al., 2009; Quan et al., 2013; Ader et al., 2014, 2016; Stüeken et al., 2016). However, the $\delta^{15}N$ can be altered during diagenesis and metamorphism to some extent (Robinson et al., 2012; Ader et al., 2016). The $\delta^{15}N$ values can be elevated by 3‰–5‰ under oxic diagenesis (Lehmann et al., 2002; Robinson et al., 2012), but the $\delta^{15}N$ values would not alter or only decrease slightly (~1‰) due to anaerobic degradation of organic matter under anoxic conditions (Freudenthal et al., 2001; Lehmann et al., 2002; Möbius et al., 2010; Robinson et al., 2012). During the metamorphism, isotopically light N would preferentially escape, resulting in higher $\delta^{15}N$ in residual N reservoirs (Ader et al., 2014). The N geochemical signals in sediments can also be influenced by continental input, but the detrital components in the Datangpo Fm were sourced from flood basalt weathering (Yu et al., 2016), and no significant relationship was found between Al_2O_3 and $\delta^{15}N$ in the Datangpo Fm (Wu et al., 2024); thus, the input of continental N was limited in the first member of the Datangpo Fm.

Nitrogen can be preserved in rocks as two forms, i.e., organic N in organic matter and ammonium (NH_4^+) bound with clay minerals. Up to 60% of sedimentary N can be bound with clays as NH_4^+ within the sediments (Müller, 1977). The positive relationship between TOC and TN indicates that N is sourced from marine primary organic matter (Calvert, 2004), while the weak or no relationship indicates inorganic clay-bound N or reflects terrigenous inputs (Calvert, 2004; Bristow et al., 2009). NH_4^+ has a similar charge and size to K^+, which can substitute for K^+ in phyllosilicates (Müller, 1977; Freudenthal et al., 2001) after being released through the degradation of organic matter (Busigny and Bebout, 2013; Stüeken et al., 2016). In this study, TOC and TN show no relationship (Figure 4A), but K_2O and TN show positive relationships in the Mn-carbonate unit [$r = +0.92$, $p(\alpha) < 0.001$] and the black shale unit [$r = +0.66$, $p(\alpha) < 0.01$] (Figure 4B), indicating that the N in sediments was bound with silicate, which were transferred from organic matter.

During the burial diagenesis and metamorphism, organic N can be preferentially lost over organic carbon, resulting in higher C/N ratios. The Datangpo Fm did not experience metamorphism; thus, the metamorphic influence on $\delta^{15}N$ can be negligible (Tu et al., 2024; Wu et al., 2024). C/N shows no relationship with $\delta^{15}N$ in the study units (Figure 4C), indicating that the preferential loss of N during burial diagenesis did not alter the $\delta^{15}N$ values (Cremonese et al., 2013). However, TN shows negative relationships with $\delta^{15}N$ [$r = -0.66$, $p(\alpha) < 0.01$] (Figure 4D) and C/N [$r = -0.87$, $p(\alpha) < 0.001$] (Figure 4E) in the Mn-carbonate unit, but no relationships in the

10.3389/fmars.2024.1469283

TABLE 1 Geochemical data of the drillcore ZK2115 in Gaodi Deposit, Guizhou Province.

Formation	Sample no.	Depth	TN	$\delta^{15}N$	$\delta^{13}C_{carb}$	$\delta^{18}O$	$\delta^{13}C_{org}$	TOC	K_2O	Mn	C/N
		(m)	(%)	(‰)	(‰)	(‰)	(‰)	(%)	(%)	(%)	
Datangpo Fm	ZK2115-H49	1,597.40	0.07	3.54			−30.80	1.0	3.2	0.2	16.9
Black shale unit	ZK2115-H47	1,599.40	0.08	3.52			−30.55	1.2	3.0	0.2	17.7
	ZK2115-H45	1,601.40	0.08	0.23			−30.91	1.3	2.9	0.1	20.8
	ZK2115-H43	1,603.40	0.09	−3.74			−30.97	1.9	3.3	0.1	25.6
	ZK2115-H41	1,605.40	0.08	1.24			−30.92	2.9	3.1	0.2	41.8
	ZK2115-H39	1,607.40	0.08	1.45			−31.11	3.1	3.3	0.4	44.2
	ZK2115-H35	1,611.40	0.08	1.85			−31.92	2.7	3.5	0.5	39.5
	ZK2115-H33	1,613.40	0.07	0.53			−31.21	1.9	4.0	0.3	30.9
	ZK2115-H31	1,615.40	0.10	1.54			−31.22	1.3	4.7	0.2	15.8
	ZK2115-H29	1,617.40	0.08	1.30			−31.64	1.7	4.1	0.3	24.4
	ZK2115-H27	1,619.40	0.10	1.75			−31.33	1.7	4.1	0.4	20.0
	ZK2115-H25	1,621.40	0.08	−0.61			−31.70	1.6	4.0	0.2	22.0
	ZK2115-H23	1,623.40	0.09	1.33			−31.26	1.8	4.4	0.2	22.6
	ZK2115-H21	1,625.40	0.09	−1.54				1.6	4.4	0.2	19.3
Datangpo Fm	ZK2115-H19	1,627.40	0.07	3.22	−5.42	−8.91	−31.95	1.6	3.4	5.7	25.4
Mn-carbonate unit	WX-32	1,627.90	0.04		−9.55	−8.17		2.8	1.3	18.3	80.3
	ZK2115-H18	1,628.40	0.05	4.77	−7.25	−9.32	−32.81	2.1	1.2	18.1	49.4
	WX-33	1,628.90	0.05	4.06				2.6	0.6	24.5	63.0
	ZK2115-H17	1,629.40	0.07	3.87	−7.05	−7.64	−32.22	1.8	3.0	9.7	28.9
	WX-34	1,629.90	0.04		−8.21	−9.55	−32.55	2.6	0.5	22.8	81.3
	ZK2115-H16	1,630.40	0.10	2.72	−7.48	−10.41	−32.85	2.0	4.1	0.9	23.2
	WX-35	1,630.90	0.04		−8.50	−10.25	−33.11	2.7	0.6	24.0	76.0
	ZK2115-H15	1,631.40	0.09	2.04			−33.19	2.9	3.0	0.9	38.8
	WX-36	1,631.70	0.12	2.67	−7.41	−9.02	−32.39	1.6	5.5	2.8	14.9
	ZK2115-H14	1,632.00	0.03		−9.25	−9.15	−33.47	2.6	0.5	26.1	107.5
	ZK2115-H13	1,632.40	0.06	3.78	−8.82	−9.38	−33.21	2.3	2.1	14.2	44.5

(Continued)

TABLE 1 Continued

Formation	Sample no.	Depth (m)	TN (%)	$\delta^{15}N$ (‰)	$\delta^{13}C_{carb}$ (‰)	$\delta^{18}O$ (‰)	$\delta^{13}C_{org}$ (‰)	TOC (%)	K_2O (%)	Mn (%)	C/N
	ZK2115-H12	1,632.80	0.08	3.69	−5.22	−6.12	−31.82	2.1	3.1	8.5	31.2
	ZK2115-H11	1,633.10	0.02	5.26	−8.78	−9.41	−32.62	1.1	0.3	24.5	64.1
	ZK2115-H10	1,633.40	0.08	4.95	−8.69	−8.14	−33.16	2.2	0.7	24.9	31.2
	ZK2115-H9	1,633.70	0.04	3.29	−9.69	−7.41	−33.09	2.6	1.2	19.9	73.0
	ZK2115-H8	1,634.10	0.08	1.53			−32.40	3.1	4.1	0.2	43.0
	ZK2115-H7	1,634.60	0.02	4.17	−8.97	−9.72	−33.61	2.5	0.3	26.9	128.6
	ZK2115-H6	1,635.10	0.11	2.57	−6.71	−8.52	−32.66	2.2	4.1	7.9	24.6
	ZK2115-H5	1,635.40	0.10	2.93	−7.97	−10.36	−32.58	2.2	4.2	2.2	25.6
	ZK2115-H4	1,635.70	0.02		−9.41	−4.81	−33.22	1.7	0.8	22.4	78.1
	ZK2115-H3	1,636.25	0.03		−10.40	−7.70	−33.31	1.9	0.7	23.1	80.0
	ZK2115-H2	1,636.55	0.03		−11.17	−7.46	−33.32	2.3	0.8	21.2	99.7
	ZK2115-H1	1,637.15	0.09	1.67			−32.96	2.4	4.2	0.4	30.7

TOC, K_2O, and Mn contents of whole rock samples are from Wang et al. (2019b, 2020).

10.3389/fmars.2024.1469283

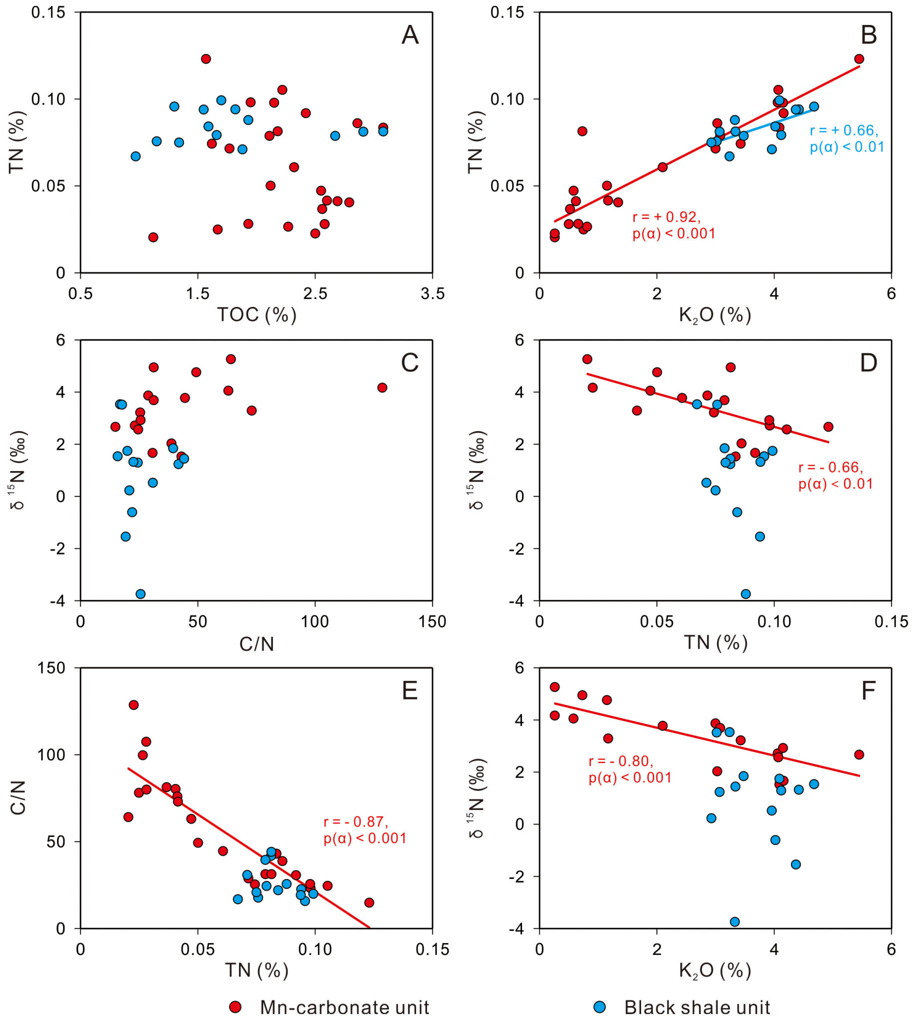

FIGURE 4
Cross-plots of TOC-TN **(A)**, K_2O-TN **(B)**, C/N-$\delta^{15}N$ **(C)**, TN-$\delta^{15}N$ **(D)**, TN-C/N **(E)**, and K_2O-$\delta^{15}N$ **(F)** in the Mn-carbonate unit (red color) and the overlying black shale unit (blue color) of the Datangpo Fm in the drillcore ZK2115. TOC and K_2O contents are collected from Wang et al. (2019b, 2020).

black shale unit (Figures 4D, E). Furthermore, the K_2O and $\delta^{15}N$ show a negative relationship in the Mn-carbonate unit [$r = -0.80$, $p(\alpha) < 0.001$], but no relationship in the black shale unit (Figure 4F). These findings indicated that the N signals were altered by early diagenesis in the Mn-carbonate unit, but the initial signals were preserved in the black shale unit.

The sedimentary carbonates record contemporaneous paleo-ocean chemistry and can be used to reflect ancient ocean information. However, carbonates are susceptible to post-depositional diagenesis, which can overprint primary geochemical signals, such as the concentrations of trace element (Mn, Fe, Ca, and Sr) and isotope compositions ($\delta^{13}C$ and $\delta^{18}O$) (e.g., Swart, 2015; Swart and Oehlert, 2018; Reis et al., 2019). Considering that Ca and Sr can be replaced by Fe and Mn from carbonate lattice during diagenesis, the elemental ratios, such as Mn/Sr and Fe/Sr, can be used to identify diagenetic alteration (e.g., Banner and Hanson, 1990; Kaufman and Knoll, 1995; Kouchinsky et al., 2008; Swart, 2015). The sediments in the Mn-carbonate unit of the Datangpo Fm were affected by strong hydrothermal activity, which can provide extra Mn and Fe to the sediments (Wu et al., 2016; Tan et al., 2021; Li et al., 2022); thus, the element ratios cannot be used to reflect diagenetic alteration in this study.

Diagenesis can also decrease the original $\delta^{13}C$ and $\delta^{18}O$ values in carbonates (e.g., Kaufman and Knoll, 1995; Melezhik et al., 2005; Derry, 2010; Swart, 2015; Reis et al., 2019), and the $\delta^{18}O$ values are more sensitive to diagenetic alterations (e.g., Banner and Hanson, 1990; Kaufman et al., 1991; Ray et al., 2003; Swart, 2015). When $\delta^{18}O > -10‰$, it indicates a small effect of diagenesis (Kaufman and Knoll, 1995). Meanwhile, the positive correlation between $\delta^{13}C_{carb}$ and $\delta^{18}O$ values is another sensitive indicator of diagenetic alterations (e.g., Kaufman and Knoll, 1995; Knauth and Kennedy, 2009; Derry, 2010; Bishop et al., 2014; Swart, 2015; Swart and Oehlert, 2018). In recent studies, the correlation between $\delta^{13}C_{org}$ and $\delta^{13}C_{carb}$ values is also used to evaluate the influence of diagenesis. If sedimentary carbonates are not influenced by meteoric water (Oehlert and Swart, 2014), the covaried $\delta^{13}C_{org}$ and $\delta^{13}C_{carb}$ values are thought to retain original carbon isotope records (e.g., Knoll et al., 1986; Johnston et al., 2012; Meyer et al., 2013). In this study, the $\delta^{18}O$ values of most samples in the Mn-carbonate unit are higher than −10‰, the $\delta^{13}C_{carb}$ and $\delta^{18}O$ values show no relationship (Figure 5A), and the $\delta^{13}C_{org}$ and $\delta^{13}C_{carb}$ values show a strong positive correlation [$r = + 0.85$, $p(\alpha) < 0.001$] (Figure 5B), implying that the $\delta^{13}C_{carb}$ values are not altered by diagenesis. Based on the diagenetic indicators, the Mn-carbonate unit recorded original carbon isotope signals and can be used to trace paleo-ocean geochemical information.

5.2 Redox conditions of the deep basin and constraints on manganese mineralization in the Cryogenian Nanhua Basin

Nitrogen has multiple valence states (−3 to +5) and is preserved as different types depending on redox conditions (Ader et al., 2014, 2016; Sigman et al., 2009; Canfield et al., 2010; Stüeken et al., 2016). The nitrogen species are complex, including nitrate, nitrite, ammonium, and N_2. The transformation between different species occur through different pathways, such as N_2 fixation, nitrification, denitrification, and anammox, which are accompanied by different N isotope fractionations (i.e., $\delta^{15}N_{product} - \delta^{15}N_{reactant}$). As atmospheric N_2 cannot be directly utilized by most living organisms, N_2 fixation by aerobic or anaerobic autotrophs (nitrogen fixers) is the only pathway for atmospheric N_2 to enter the marine N cycle. Atmospheric N_2 is transferred to organic matter as NH_4^+ through N_2 fixation, and this process generates minor N isotope fractionation (−2‰ to +1‰), except under Fe^{2+}-enriched conditions or in thermophilic cultures where it can reach −4‰ (Zerkle et al., 2008; Stüeken et al., 2016). Bioavailable N in the ocean (e.g., NH_4^+ and NO_3^-) is originally sourced from organic matter. Nitrification, which can transfer NH_4^+ to NO_3^-, occurs under oxic conditions. When NH_4^+ is partially oxidized, the residual NH_4^+ is enriched with ^{15}N. Denitrification occurs in anoxic water columns and sediments, and can transfer NO_3^- to N_2. When NO_3^- is completely consumed, the N isotope generates no isotope fractionation. However, when NO_3^- is not completely consumed in the water columns, ^{14}N-enriched NO_3^- is preferentially reduced, resulting in significant N isotope fractionation (~−20% to −30%; Sigman et al., 2009). The N isotope fractionation during denitrification that occurs under anoxic sediments is negligible, because NO_3^- is completely consumed in porewater (Sigman et al., 2009; Cremonese et al., 2013). Anammox occurs under strictly anoxic conditions, and N_2 is generated through the reaction of NH_4^+ and NO_2^-. This is another important pathway by which N is lost from the ocean N cycle.

In the Mn-carbonate unit and the black shale unit of the Datangpo Fm, N was bound to silicates, which was sourced from organic matter. N was initially preserved in organic matter as NH_4^+ and formed through N_2 fixation. The $\delta^{15}N$ values of organic matter N were low, because of the minor N isotope fractionation during this process and the low $\delta^{15}N$ values of atmospheric N_2 (0‰). During the sinking of the generated organic matter into the sediments, the oxidation processes almost had no effect on the N-bearing biomass (Wu et al., 2024). When NH_4^+ was released from organic matter during organic matter mineralization, there was small isotope fractionation owing to its efficiency (Möbius, 2013). If the released NH_4^+ remains stable under anoxic conditions, N isotope fractionation during non-quantitative NH_4^+ assimilation can be significant ($\Delta_{org-NH4+}$: up to −27‰) when $[NH_4^+]$ is greater than 20 µM, resulting in ^{15}N-depleted organic matter (Pennock et al.,1996; Stüeken et al., 2016), but it decreases strongly as the availability of NH_4^+increases, and no fractionation is generated when it is completely consumed. The elevated $\delta^{15}N$ values in sediments throughout Earth's history might be related to intense denitrification under suboxic conditions, compared with the relatively low $\delta^{15}N$ values recorded under oxic and anoxic conditions (e.g., Quan et al., 2013), but other studies attributed this to oxic diagenesis (Stüeken et al., 2016). When the released NH_4^+ was partially oxidized under oxic conditions, oxidation rate was rapid, and ^{14}N was preferential oxidized, resulting in residual NH_4^+ characterized by higher $\delta^{15}N$ values. The nitrification of NH_4^+ generated the highest $\delta^{15}N$ in sediments at ~2.7 Ga (up to +50‰; Thomazo et al., 2011). Considering the changes in TN and $\delta^{15}N$ during early diagenesis, the deep water was probably oxic during the precipitation of the Mn-carbonate unit, which can result in a negative relationship between TN and $\delta^{15}N$ (Figure 4D), whereas the deep water was anoxic during the precipitation of the black shale unit.

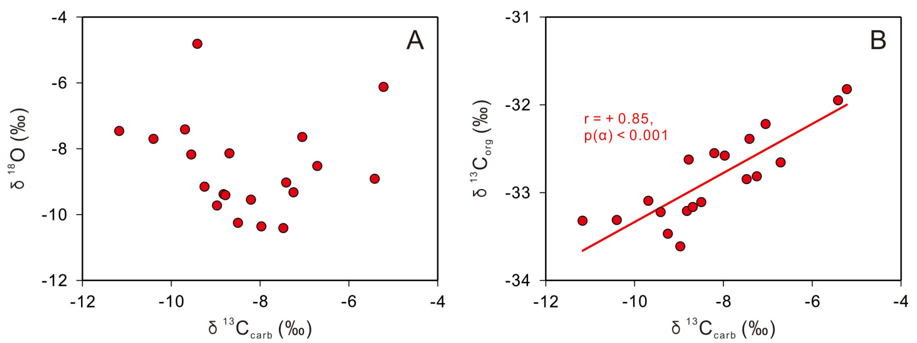

FIGURE 5
Cross-plots of $\delta^{13}C_{carb}$-$\delta^{18}O$ **(A)** and $\delta^{13}C_{carb}$-$\delta^{13}C_{org}$ **(B)** in the Mn-carbonate unit of the Datangpo Fm in the drillcore ZK2115.

In the Mn-carbonate unit of the Datangpo Fm, the Mn contents show a strong negative relationship with TN [$r = -0.86$, $p(\alpha) < 0.001$] (Figure 6A), but a positive relationship with $\delta^{15}N$ [$r = +0.85$, $p(\alpha) < 0.001$] (Figure 6B), implying that the metallogenesis of the manganese deposits was related to N geochemical signals. When large amounts of Mn-carbonates were reduced from Mn-oxides/oxyhydroxides, abundant organic matter can be degraded, accompanied by enhanced release of NH_4^+. However, low contents of N and ^{15}N-enriched NH_4^+ were transferred to silicate, indicating that ^{14}N-enriched NH_4^+ was preferentially consumed, which may be related to oxic conditions in the deep basin. Under oxic conditions, significant N isotope fractionation can occur when NH_4^+ was partially oxidized, resulting in residual NH_4^+ characterized by relatively higher $\delta^{15}N$ values.

The redox conditions in the deep Nanhua Basin are not clear in the basal Datangpo Fm. For example, Fe speciation in the Mn-carbonate unit of the Datangpo Fm recorded oxic intervals in the Yangjiaping section (Li et al., 2012), but anoxic conditions in the Xiushan section (Ma et al., 2019), Gaodi and Xixibao sections (Cheng et al., 2021), Daotuo and Datangpo sections (Wu et al., 2024), and the overlying black shale unit (cf. Wu et al., 2024). Additionally, C_{org}:P and Ce/Ce* recorded oxic–suboxic conditions in the Mn-carbonate unit and anoxic conditions in the black shale unit (Yu et al., 2016; Xiao et al., 2017; Ai et al., 2021). The findings of this study showed that the Mn-carbonate unit recorded oxic intervals, and the redox variations in the deep Nanhua Basin were related to the episodic ventilation by density flow, which can transfer oxygen to deep water and result in intermittent oxygenation (Yu et al., 2016). Episodic ventilation facilitated the metallogenesis of the manganese deposits in the Nanhua Basin, and the dissolved Mn^{2+} was first oxidized to Mn-oxides/oxyhydroxides in the oxic deep Nanhua Basin, which were reduced and ultimately preserved as Mn-carbonates in the sediments (Yu et al., 2016, 2017; Wu et al., 2016; Xiao et al., 2017).

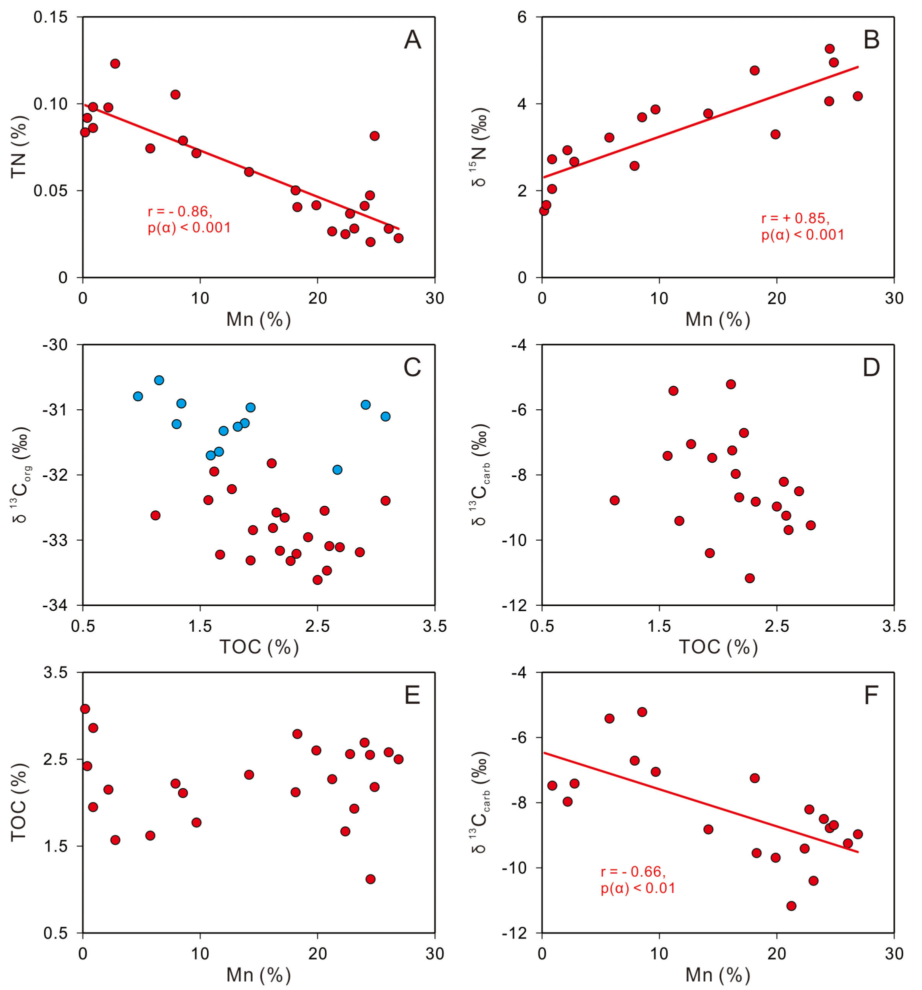

FIGURE 6
Cross-plots of Mn-TN **(A)**, Mn-$\delta^{15}N$ **(B)**, TOC-$\delta^{13}C_{org}$ **(C)**, TOC-$\delta^{13}C_{carb}$ **(D)**, Mn-TOC **(E)**, and Mn-$\delta^{13}C_{carb}$ **(F)** in the Mn-carbonate unit (red color) and the overlying black shale unit (blue color) of the Datangpo Fm in the drillcore ZK2115. TOC and Mn contents are collected from Wang et al. (2019b).

5.3 Anomalous $\delta^{13}C_{carb}$ excursions in the post-Sturtian Nanhua Basin, South China

5.3.1 Carbon isotope evolution of organic matter after the Sturtian Glaciation

Based on the Snowball Earth hypothesis (Kirschvink, 1992; Hoffman et al., 1998; Hoffman and Schrag, 2002), the ice sheet prevailed on Earth during Neoproterozoic global glaciations, and even reached the equator. However, the ecosystem did not completely collapse during the extreme icehouse climate. For example, the evidence of organic molecules and biomarkers indicates that photosynthesis never ceased during the Sturtian Glaciation, even though the rate was low (Olcott et al., 2005; Wang et al., 2008; Riedman et al., 2014). The organic matter generated through photosynthesis was preserved in glacial sediments, which were characterized by low TOC contents (mean 0.12%; McKirdy et al., 2001; Olcott et al., 2005; Pei et al., 2020).

After the Sturtian Glaciation, the ice sheet melted, accompanied by a transition from icehouse climate to greenhouse climate (Hoffman et al., 1998; Yonkee et al., 2014; Scheller et al., 2018), and the chemical weathering intensity was enhanced, leading to the transfer of large amounts of nutrients into the ocean (e.g., Rieu et al., 2007; Zhu et al., 2019; Ai et al., 2020a; Wang et al., 2020; Wei et al., 2020; Li et al., 2022). At the end of the Sturtian Glaciation, microbes began to flourish (e.g., Zhu et al., 2019; Ai et al., 2020b). The planktonic biotas were widespread and abundant after the glaciation (Riedman et al., 2014). Moreover, the rise of algae (including cyanobacteria) with great diversities contributed to the organic matter inputs in the post-Sturtian sediments (Brocks et al., 2017; Zhu et al., 2019; Ai et al., 2020b). In the Nanhua Basin, the post-Sturtian Datangpo Fm sediments were strongly affected by hydrothermal activity (Wu et al., 2016; Yu et al., 2016; Tan et al., 2021; Li et al., 2022), which can also provide essential nutrients for life in the ocean, promoting microbial breeding and increasing the rate of photosynthesis (Tribovillard et al., 2006; Dick et al., 2013).

In this study, the Mn-carbonate unit and the black shale unit of the Datangpo Fm are characterized by high TOC contents (mean 2.2% and 1.8%, respectively; Wang et al., 2019b) (Figure 3), which are consistent with previous studies in this basin (Figure 7; e.g., Wei et al., 2016; Zhu et al., 2019, 2022; Ai et al., 2020a, 2021; Tan et al., 2021; Li et al., 2022; Zhao et al., 2022). The high TOC contents were also recorded in the coeval clastic sedimentary sequences, such as the Twitya Fm in Canada (Sperling et al., 2016), the Arena Fm in East Greenland (Scheller et al., 2018), the MacDonaldryggen Member of the Elbobreen Fm in Svalbard (Kunzmann et al., 2015), and the Tapley Hill Fm and Aralka Fm in Australia (McKirdy et al., 2001; Bowyer et al., 2023). The TOC contents show a decreasing trend from the Mn-carbonate unit and black

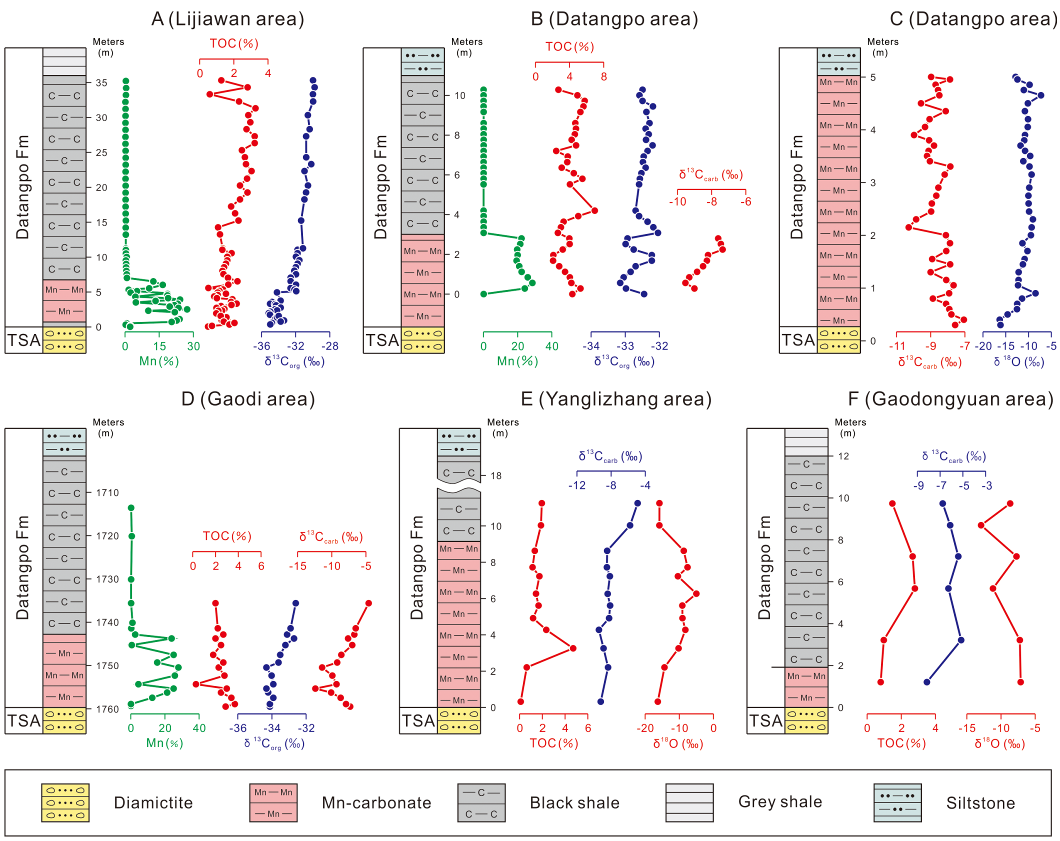

FIGURE 7
Mn, TOC, and $\delta^{13}C$ profiles for first member of the Datangpo Fm of Lijiawan area (**A**; Li et al., 2022), Datangpo area (**B, C**; Zhou et al., 2007; Tan et al., 2021), Gaodi area (**D**; Pei et al., 2020), and Yanglizhang area (**E**; Zhu et al., 2019) in Guizhou Province and Gaodongyuan area in Chongqing City (**F**; Zhu et al., 2019). TSA, Tiesi'ao Fm.

shale unit to the overlying gray shales (only discovered in limited areas) and the second member of the Datangpo Fm (mean 0.25% and 0.12%, respectively; Li et al., 2012; Peng et al., 2019; Zhu et al., 2019, 2022; Shen et al., 2022). This finding may be related to the elevated oxygenated environment and rapid deposition rates, which were not conducive to the preservation of organic matter (Zhu et al., 2019). Whether the organic matter preserved in the sediments was derived from primary productivity through photosynthesis needs to be further studied. The detrital materials of the first member of the Datangpo Fm were sourced from weathering of continental flood basalts (Yu et al., 2016; Ai et al., 2020a), and the amount of recycled organic matter input from continents was small; thus, this kind of organic matter in the Datangpo Fm can be ignored (Burdige, 2007; Peng et al., 2019). Thermal maturation during diagenetic or metamorphic processes preferentially removes the light isotopic composition for organic carbon isotopes, resulting in negative correlations between the TOC and $\delta^{13}C_{org}$ values (Clayton, 1991; Hayes et al., 1999), but the TOC and $\delta^{13}C_{org}$ values in the study sections show no relationship (Figure 6C), indicating that the $\delta^{13}C_{org}$ values were not altered by diagenetic or metamorphic alterations. Additionally, the microbial sulfate reduction process played a significant role during the organic matter degradation, but the seawater sulfate concentration in Neoproterozoic was extremely low (Hurtgen et al., 2002; Zhao et al., 2022), implying that organic matter consumption by microbial sulfate reduction was extremely low. The above findings showed that the organic matter preserved in the Datangpo Fm was mainly the product of photosynthesis after the glaciation and recorded the original carbon isotope signals.

The carbon isotope compositions of organic matter show a gradually increasing trend from the Mn-carbonate unit (mean −32.46‰) to the overlying black shale unit (mean −31.20‰) (Figures 3, 7), and this shift can also be observed in other sections across the Nanhua Basin (e.g., Wei et al., 2016; Ai et al., 2020a, 2021; Pei et al., 2020; Tan et al., 2021; Li et al., 2022). The high-resolution $\delta^{13}C_{org}$ values also show an increasing tendency in the complete Datangpo Fm between the Sturtian and Marinoan glaciations (Peng et al., 2019; Zhu et al., 2022; Bowyer et al., 2023), which was consistent with the MacDonaldryggen Member of the Elbobreen Fm in Svalbard (ca. −34.0‰ to −30.4‰, Halverson, 2011; Ader et al., 2014) and the Arena Fm in East Greenland (−33.7‰ to −30.7‰, Scheller et al., 2018). The increasing $\delta^{13}C_{org}$ values in the post-glacial sediments may be related to the burial of large amounts of organic matter. During photosynthesis, the lighter ^{12}C was preferentially utilized and incorporated into organic matter, resulting in low $\delta^{13}C$ values of organic matter. With the increasing burial of organic matter into post-glacial sediments, large amounts of ^{12}C were fixed in the sediments, resulting in higher carbon isotope compositions of organic matter generated in later stages. Therefore, the long-term organic carbon isotope evolution in the post-Sturtian interval was related to the burial of organic matter generated through photosynthesis.

5.3.2 The negative $\delta^{13}C_{carb}$ excursions in the manganese deposits of the Nanhua Basin

The Mn-carbonate unit of the Datangpo Fm is characterized by negative carbon isotope excursions, ranging from −11.17‰ to −5.22‰ with a mean of −8.30‰ (Figure 3), similar to the carbon isotope compositions of coeval manganese deposits in the Nanhua Basin, such as Datangpo, Xiushan, Gucheng, and Xiangtan manganese deposits (Figure 7; e.g., Li et al., 1999; Zhou et al., 2007; Chen et al., 2008; Wu et al., 2016; Qu et al., 2018; Zhu et al., 2019; Pei et al., 2020; Tan et al., 2021; Dong et al., 2023). The $\delta^{13}C_{carb}$ values of the Mn-carbonate unit are lower than those of the overlying black shale unit in South China (−6.76‰ to −5.15‰, mean −5.94‰; Zhu et al., 2019) (Figure 7F) and coeval marine clastic sediments globally, such as the Arena Fm shales in East Greenland (−7.88‰ to +1.42‰, mean −3.39‰, n = 18; Scheller et al., 2018) and the Tindelpina Shale Member of the Tapley Hill Fm in South Australia (−6.7‰ to +1.5‰, mean −3.59‰, n = 39; McKirdy et al., 2001; Giddings and Wallace, 2009). However, the $\delta^{13}C_{carb}$ values of the basal Datangpo Fm are lower than the carbon isotope compositions of the mantle (−5‰; Kump and Arthur, 1999); thus, the influence of the mantle on the negative carbon isotope excursions can be excluded. Many studies suggested that this phenomenon was related to organic matter degradation, which can provide ^{13}C-depleted carbon (Li et al., 1999; Chen et al., 2008; Wu et al., 2016; Qu et al., 2018; Zhu et al., 2019). The TOC and $\delta^{13}C_{carb}$ show no relationship (Figure 6D), indicating that the inorganic carbon isotope compositions of the Mn-carbonates were not influenced by the TOC contents. Meanwhile, the Mn contents show no relationship with TOC (Figure 6E), but a negative relationship with $\delta^{13}C_{carb}$ [r = −0.66, $p(\alpha) < 0.01$] (Figure 6F), implying that the organic matter was sufficient for the Mn reduction and that the $\delta^{13}C_{carb}$ values were influenced by Mn-carbonate formation. The elevated Mn-carbonate formation indicated enhanced organic matter mineralization, resulting in more ^{12}C-enriched C being transferred to CO_3^{2-} and ultimately preserved in Mn-carbonates, which were characterized by lower $\delta^{13}C_{carb}$ values. Therefore, the negative carbon isotope excursions in the post-Sturtian Nanhua Basin were related to the metallogenic process of the manganese deposits, similar to the Ediacaran manganese deposits in the northern margin of the Yangtze Block (Zhang et al., 2024a, 2024b). These lines of evidence also suggested that the Mn-carbonates were mainly precipitated with the precursor of Mn-oxides/oxyhydroxides (Yu et al., 2016, 2017; Wu et al., 2016; Xiao et al., 2017). However, a previous study suggested that part of Mn-carbonates can precipitate directly from anoxic water columns, which are characterized by small grains (<2 μm) and core–shell structures (i.e., a minor Ca-carbonate core enclosed by a Mn-carbonate shell) (Ai et al., 2023). This process of Mn-carbonate formation can occur when the deep basin was episodic anoxic, but it is not the major metallogenic process. Furthermore, only small amounts of Mn-carbonates can be formed through this process.

5.4 N–C cycling in the post-Sturtian Nanhua Basin, South China

Based on this study, we propose a new nitrogen and carbon cycling model for the post-Sturtian Nanhua Basin. During the Sturtian Glaciation, photosynthesis rates were relatively weak during extreme icehouse climate, and the recorded OM contents in glacial sediments were low (mean 0.12%; McKirdy et al., 2001; Olcott et al., 2005; Pei et al., 2020). After the Sturtian Glaciation, the ice sheet melted accompanied by the transition to greenhouse climate. The ecosystem recovered, photosynthesis rates increased dramatically, and ^{12}C was preferentially utilized and incorporated into the organic matter during this process (Knauth and Kennedy, 2009). Large amounts of organic matter generated by photosynthesis were preserved in the Mn-carbonate unit of the Datangpo Fm, which was characterized by high TOC contents (mean 2.2%) with a mean $\delta^{13}C_{org}$ of −32.84‰ (Figure 8A). During the formation of organic matter, atmospheric N_2 was fixed in organic matter as NH_4^+. The organic matter (including N_{org}) then sank into the sediments. During the postglacial interval, episodic ventilation in the deep Nanhua Basin transferred large amounts of oxygen into the deep basin (Feng et al., 2010; Li et al., 2012; Yu et al., 2016; Dong et al., 2023), which led to intermittent oxic conditions in the deep Nanhua Basin. Hydrothermally sourced Mn^{2+} was oxidized to Mn-oxides/oxyhydroxides and then reduced to Mn-carbonates after being co-buried with organic matter in the sediments (Yu et al., 2016, 2017; Wu et al., 2016; Xiao et al., 2017). During this process, organic matter acted as an electron acceptor and facilitated the reduction of Mn-oxides/oxyhydroxides. During early diagenesis, N_{org} was preferentially released over C_{org}. Moreover, N_{org} was released as NH_4^+ from organic matter, part of which was oxidized to NO_3^- in the oxic deep basin, and significant N isotope fractionations were generated during this process. This residual NH_4^+ was bound with silicates and characterized by elevated $\delta^{15}N$ values (mean +3.36‰). During organic matter mineralization driven by Mn-carbonate formation, ^{13}C-depleted C led to negative $\delta^{13}C_{carb}$ excursions (mean −8.30‰).

During the deposition of the black shale unit of the Datangpo Fm, the photosynthesis rates were still high, and the sediments were also characterized by high TOC contents (mean 1.8%) (Figure 8B). With the burial of ^{13}C-depleted organic matter after the Sturtian Glaciation, the latterly formed organic matter was characterized by higher carbon isotope compositions (mean −31.20‰), which caused the $\delta^{13}C_{org}$ values in the black shale unit to be higher than the Mn-carbonate unit and show an increasing trend during the postglacial interval (Figure 3). During this period, the deep water was anoxic and covered by oxic surface water. After the OM (including N_{org}) sank, NH_4^+ was released from the organic matter, part of which diffused into anoxic deep water without N isotope fractionation. The residual NH_4^+ was bound to silicate, which recorded the original $\delta^{15}N$ signals (mean +0.89‰). Moreover, the seawater DIC reservoir in the black shale unit inherited the carbon isotope compositions of the Mn-carbonate unit, but the organic matter degradation facilitated by Mn-carbonate formation ceased; thus, the ^{13}C-depleted carbon input was lacking. Therefore, the $\delta^{13}C_{carb}$ values in sediments showed negative $\delta^{13}C_{carb}$ excursions (mean −5.81‰; Zhu et al., 2019; Pei et al., 2020) but were greater than the underlying Mn-carbonate unit (mean −8.30‰).

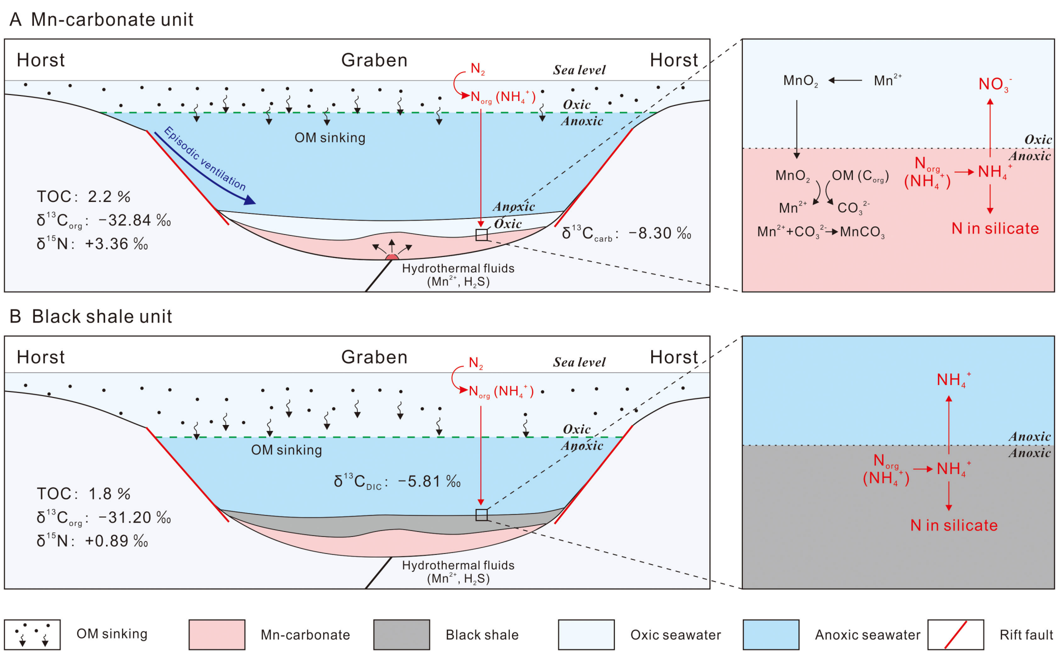

FIGURE 8
Nitrogen and carbon cycling model in the Mn-carbonate unit **(A)** and the black shale unit **(B)** of the Datangpo Fm after the Sturtian Glaciation.

6 Conclusions

The Nanhua Basin of South China recorded the complete Cryogenian stratigraphic sequence from the Sturtian to the Marinoan glaciations, and the manganese deposits precipitated in the interglacial Datangpo Fm. The main findings of this study are as follows:

1. After the Sturtian Glaciation, the Mn-carbonate unit is characterized by relatively high $\delta^{15}N$ values (mean +3.66‰), implying the oxic conditions in the Mn-carbonate unit. The oxic deep basin facilitated the Mn^{2+} oxidation to Mn-oxides/oxyhydroxides, which were ultimately reduced and preserved as Mn-carbonates in the sediments. Therefore, the metallogenic process of the manganese deposits was mainly constrained by redox variations, which experienced two stages. The overlying black shale unit is characterized by relatively low $\delta^{15}N$ values (mean +0.89‰), indicating the anoxic conditions during this period.
2. During the reduction of Mn-oxides/oxyhydroxides, organic matter was mineralized, resulting in ^{13}C-depleted CO_3^{2-} being formed and preserved in Mn-carbonates. The Mn-carbonate unit recorded the negative $\delta^{13}C_{carb}$ excursions (mean −8.30‰), which were caused by the Mn-carbonate formation. Carbon cycling in the deep Nanhua Basin was strongly affected by the metallogenesis of the Cryogenian manganese deposits.
3. The nitrogen and carbon cycling processes in the post-Sturtian Nanhua Basin were influenced by redox variations, and the N–C cycling model in the Cryogenian Nanhua Basin was reconstructed. This model can also provide new insights for the biogeochemical cycling in other ocean systems.

Data availability statement

The original contributions presented in the study are included in the article/supplementary material. Further inquiries can be directed to the corresponding author.

Author contributions

PW: Writing – original draft, Writing – review & editing. JW: Writing – original draft. YD: Writing – review & editing. WY: Writing – review & editing. QZ: Writing – review & editing. LT:Writing – review & editing. LY: Writing – review & editing. WP: Writing – review & editing. WW: Writing – review & editing. YQ: Writing – review & editing. ZM: Writing – review & editing.

Funding

The author(s) declare financial support was received for the research, authorship, and/or publication of this article. This work was supported by the National Natural Science Foundation of China (No. 42202111), the Open Research Program of State Key Laboratory of Biogeology and Environmental Geology, China University of Geosciences (Wuhan) (No. GBL22107), the Postdoctoral Foundation and Key Scientific Research Project of Henan Province, China (No. HN2022027 and No. 24A170019), and the Open Fund of Engineering Technology Innovation Center of Mineral Resources Explorations in Bedrock Zones, Ministry of Natural Resources (No. MREBZ-2023-OF01).

Acknowledgments

We thank the editors and reviewers for their constructive comments. We are grateful to the officers of China University of Geosciences (Wuhan) for the lab work.

Conflict of interest

The authors declare that the research was conducted in the absence of any commercial or financial relationships that could be construed as a potential conflict of interest.

Publisher's note

References

Ader, M., Sansjofre, P., Halverson, G. P., Busigny, V., Trindade, R. I., Kunzmann, M., et al. (2014). Ocean redox structure across the Late Neoproterozoic Oxygenation Event: a nitrogen isotope perspective. *Earth Planet. Sci. Lett.* 396, 1–13. doi: 10.1016/j.epsl.2014.03.042

Ader, M., Thomazo, C., Sansjofre, P., Busigny, V., Papineau, D., Laffont, R., et al. (2016). Interpretation of the nitrogen isotopic composition of Precambrian sedimentary rocks: Assumptions and perspectives. *Chem. Geol.* 429, 93–110. doi: 10.1016/j.chemgeo.2016.02.010

Ai, J. Y., George, S. C., and Zhong, N. N. (2020b). Organic geochemical characteristics of highly mature Late Neoproterozoic black shales from South China: Reappraisal of syngeneity and indigeneity of hydrocarbon biomarkers. *Precambrian Res.* 336, 105508. doi: 10.1016/j.precamres.2019.105508

Ai, J. Y., Siljeström, S., Zhong, N. N., Chen, J. F., Wang, T. G., Qiu, N. S., et al. (2023). Co-existing two distinct formation mechanisms of micro-scale ooid-like manganese carbonates hosted in Cryogenian organic-rich black shales in South China. *Precambrian Res.* 393, 107091. doi: 10.1016/j.precamres.2023.107091

Ai, J. Y., Zhong, N. N., George, S. C., Zhang, Y., Yao, L. P., and Wang, T. G. (2020a). Evolution of paleo-weathering during the late Neoproterozoic in South China: Implications for paleoclimatic conditions and organic carbon burial. *Palaeogeogr. Palaeoclimatol. Palaeoecol.* 555, 109843. doi: 10.1016/j.palaeo.2020.109843

Ai, J. Y., Zhong, N. N., Zhang, T. G., Zhang, Y., Wang, T. G., and George, S. C. (2021). Oceanic water chemistry evolution and its implications for post-glacial black shale formation: Insights from the Cryogenian Datangpo Formation, South China. *Chem. Geol.* 566, 120083. doi: 10.1016/j.chemgeo.2021.120083

Banner, J. L., and Hanson, G. N. (1990). Calculation of simultaneous isotopic and trace element variations during water-rock interaction with applications to carbonate diagenesis. *Geochim. Cosmochim. Acta* 54, 3123–3137. doi: 10.1016/0016-7037(90)90128-8

Bishop, J. W., Osleger, D. A., Montañez, I., and Sumner, D. Y. (2014). Meteoric diagenesis and fluid-rock interaction in the middle Permian capitan backreef: Yates formation, slaughter canyon, New Mexico. *AAPG Bull.* 98, 1495–1519. doi: 10.1306/05201311158

Bowyer, F. T., Krause, A. J., Song, Y. F., Huang, K. J., Fu, Y., Shen, B., et al. (2023). Biological diversification linked to environmental stabilization following the Sturtian Snowball glaciation. *Sci. Adv.* 9, eadf9999. doi: 10.1126/sciadv.adf9999

Bristow, T. F., Kennedy, M. J., Derkowski, A., Droser, M. L., Jiang, G. Q., and Creaser, R. A. (2009). Mineralogical constraints on the paleoenvironments of the Ediacaran Doushantuo Formation. *PNAS* 106, 13190–13195. doi: 10.1073/pnas.0901080106

Brocks, J. J., Jarrett, A. J., Sirantoine, E., Hallmann, C., Hoshino, Y., and Liyanage, T. (2017). The rise of algae in Cryogenian oceans and the emergence of animals. *Nature* 548, 578–581. doi: 10.1038/nature23457

Bühn, B., Stanistreet, I. G., and Okrusch, M. (1992). Late Proterozoic outer shelf manganese and iron deposits at Otjosondu (Namibia) related to the Damaran oceanic opening. *Econ. Geol.* 87, 1393–1411. doi: 10.2113/gsecongeo.87.5.1393

Burdige, D. J. (2007). Preservation of organic matter in marine sediments: controls, mechanisms, and an imbalance in sediment organic carbon budgets? *Chem. Rev.* 107, 467–485. doi: 10.1021/cr050347q

Busigny, V., and Bebout, G. E. (2013). Nitrogen in the silicate Earth: Speciation and isotopic behavior during mineral-fluid interactions. *Elements* 9, 353–358. doi: 10.2113/gselements.9.5.353

Cabral, A. R., Moore, J. M., Mapani, B. S., Koubová, M., and Sattler, C. D. (2011). Geochemical and mineralogical constraints on the genesis of the Otjosondu ferromanganese deposit, Namibia: hydrothermal exhalative versus hydrogenetic (including snowball-earth) origins. *S. Afr. J. Geol.* 114, 57–76. doi: 10.2113/gssajg.114.1.57

Calvert, S. E. (2004). Beware intercepts: interpreting compositional ratios in multi-component sediments and sedimentary rocks. *Org. Geochem.* 35, 981–987. doi: 10.1016/j.orggeochem.2004.03.001

Canfield, D. E., Glazer, A. N., and Falkowski, P. G. (2010). The evolution and future of Earth's nitrogen cycle. *Science* 330, 192–196. doi: 10.1126/science.1186120

Chen, X., Li, D., Ling, H. F., and Jiang, S. Y. (2008). Carbon and sulfur isotopic compositions of basal Datangpo Formation, northeastern Guizhou, South China: Implications for depositional environment. *Prog. Nat. Sci.* 18, 421–429. doi: 10.1016/j.pnsc.2007.10.008

Cheng, M., Zhang, Z. H., Algeo, T. J., Liu, S. L., Liu, X. D., Wang, H. Y., et al. (2021). Hydrological controls on marine chemistry in the Cryogenian Nanhua Basin (South China). *Earth-Sci. Rev.* 218, 103678. doi: 10.1016/j.earscirev.2021.103678

Clayton, C. J. (1991). Effect of maturity on carbon isotope ratios of oils and condensates. *Org. Geochem.* 17, 887–899. doi: 10.1016/0146-6380(91)90030-N

Cremonese, L., Shields-Zhou, G., Struck, U., Ling, H. F., Och, L., Chen, X., et al. (2013). Marine biogeochemical cycling during the early Cambrian constrained by a nitrogen and organic carbon isotope study of the Xiaotan section, South China. *Precambrian Res.* 225, 148–165. doi: 10.1016/j.precamres.2011.12.004

Dalziel, I. W. D. (1991). Pacific margins of Laurentia and East Antarctica-Australia as a conjugate rift pair: evidence and implications for an Eocambrian supercontinent. *Geology* 19, 598–601. doi: 10.1130/0091-7613(1991)019<0598:PMOLAE>2.3.CO;2

Derry, L. A. (2010). A burial diagenesis origin for the Ediacaran Shuram-Wonoka carbon isotope anomaly. *Earth Planet. Sci. Lett.* 294, 152–162. doi: 10.1016/j.epsl.2010.03.022

Dick, G. J., Anantharaman, K., Baker, B. J., Li, M., Reed, D. C., and Sheik, C. S. (2013). The microbiology of deep-sea hydrothermal vent plumes: ecological and biogeographic linkages to seafloor and water column habitats. *Front. Microbiol.* 4, 124. doi: 10.3389/fmicb.2013.00124

Dong, F. Y., Yin, L., Dong, Z. G., Liu, J. Y., Tan, Z. Z., Long, X. P., et al. (2023). Dynamic deep-water oxygenation of marginal seas in the aftermath of the Sturtian Snowball Earth: Insights from redox-hydrological reconstructions of the Nanhua basin (South China). *Precambrian Res.* 398, 107219. doi: 10.1016/j.precamres.2023.107219

Feng, L. J., Chu, X. L., Huang, J., Zhang, Q. R., and Chang, H. J. (2010). Reconstruction of paleo-redox conditions and early sulfur cycling during deposition of the Cryogenian Datangpo Formation in South China. *Gondwana Res.* 18, 632–637. doi: 10.1016/j.gr.2010.02.011

Freudenthal, T., Wagner, T., Wenzhöfer, F., Zabel, M., and Wefer, G. (2001). Early diagenesis of organic matter from sediments of the eastern subtropical Atlantic: evidence from stable nitrogen and carbon isotopes. *Geochim. Cosmochim. Acta* 65, 1795–1808. doi: 10.1016/S0016-7037(01)00554-3

Giddings, J. A., and Wallace, M. W. (2009). Facies-dependent $\delta^{13}C$ variation from a Cryogenian platform margin, South Australia: Evidence for stratified Neoproterozoic oceans? *Palaeogeogr. Palaeoclimatol. Palaeoecol.* 271, 196–214. doi: 10.1016/j.palaeo.2008.10.011

Gutzmer, J., and Beukes, N. J. (1998). The manganese formation of the Neoproterozoic Penganga Group, India; revision of an enigma. *Econ. Geol.* 93, 1091–1102. doi: 10.2113/gsecongeo.93.7.1091

Halverson, G. P. (2011). "Glacial sediments and associated strata of the Polarisbreen Group, northeastern Svalbard," in *The Geological Record of Neoproterozoic Glaciations*. Eds. E. Arnaud, G. P. Halverson and G. Shields-Zhou (Geological Society, London), 571–579.

Hayes, J. M., Strauss, H., and Kaufman, A. J. (1999). The abundance of ^{13}C in marine organic matter and isotopic fractionation in the global biogeochemical cycle of carbon during the past 800 Ma. *Chem. Geol.* 161, 103–125. doi: 10.1016/S0009-2541(99)00083-2

Hoffman, P. F. (1991). Did the breakout of Laurentia turn Gondwanaland inside-out? *Science* 252, 1409–1412. doi: 10.1126/science.252.5011.1409

Hoffman, P. F., Abbot, D. S., Ashkenazy, Y., Benn, D. I., Brocks, J. J., Cohen, P. A., et al. (2017). Snowball Earth climate dynamics and Cryogenian geology-geobiology. *Sci. Adv.* 3, e1600983. doi: 10.1126/sciadv.1600983

Hoffman, P. F., Kaufman, A. J., Halverson, G. P., and Schrag, D. P. (1998). A Neoproterozoic snowball earth. *Science* 281, 1342–1346. doi: 10.1126/science.281.5381.1342

Hoffman, P. F., and Schrag, D. P. (2002). The snowball Earth hypothesis: testing the limits of global change. *Terra Nova* 14, 129–155. doi: 10.1046/j.1365-3121.2002.00408.x

Hurtgen, M. T., Arthur, M. A., Suits, N. S., and Kaufman, A. J. (2002). The sulfur isotopic composition of Neoproterozoic seawater sulfate: implications for a snowball Earth? *Earth Planet. Sci. Lett.* 203, 413–429. doi: 10.1016/S0012-821X(02)00804-X

Johnston, D. T., Macdonald, F. A., Gill, B. C., Hoffman, P. F., and Schrag, D. P. (2012). Uncovering the Neoproterozoic carbon cycle. *Nature* 483, 320–323. doi: 10.1038/nature10854

Kaufman, A. J., Hayes, J. M., Knoll, A. H., and Germs, G. J. (1991). Isotopic compositions of carbonates and organic carbon from upper Proterozoic successions in Namibia: stratigraphic variation and the effects of diagenesis and metamorphism. *Precambrian Res.* 49, 301–327. doi: 10.1016/0301-9268(91)90039-D

Kaufman, A. J., and Knoll, A. H. (1995). Neoproterozoic variations in the C-isotopic composition of seawater: stratigraphic and biogeochemical implications. *Precambrian Res.* 73, 27–49. doi: 10.1016/0301-9268(94)00070-8

Kirschvink, J. L. (1992). "Late Proterozoic low-latitude global glaciation: the snowball Earth," in *The Proterozoic Biosphere: A Multidisciplinary Study*. Eds. J. W. Schopf, C. Klein and D. Des Maris (Cambridge University Press, Cambridge), 51–52.

Klein, C., and Ladeira, E. A. (2004). Geochemistry and mineralogy of Neoproterozoic banded iron-formations and some selected, siliceous manganese formations from the Urucum District, Mato Grosso do Sul, Brazil. *Econ. Geol.* 99, 1233–1244. doi: 10.2113/gsecongeo.99.6.1233

Knauth, L. P., and Kennedy, M. J. (2009). The late Precambrian greening of the Earth. *Nature* 460, 728–732. doi: 10.1038/nature08213

Knoll, A. H., Hayes, J. M., Kaufman, A. J., Swett, K., and Lambert, I. B. (1986). Secular variation in carbon isotope ratios from Upper Proterozoic successions of Svalbard and East Greenland. *Nature* 321, 832–838. doi: 10.1038/321832a0

Kouchinsky, A., Bengtson, S., Gallet, Y., Korovnikov, I., Pavlov, V., Runnegar, B., et al. (2008). The SPICE carbon isotope excursion in Siberia: a combined study of the upper Middle Cambrian–lowermost Ordovician Kulyumbe River section, northwestern Siberian Platform. *Geol. Mag.* 145, 609–622. doi: 10.1017/S0016756808004913

Kump, L. R., and Arthur, M. A. (1999). Interpreting carbon-isotope excursions: carbonates and organic matter. *Chem. Geol.* 161, 181–198. doi: 10.1016/S0009-2541(99)00086-8

Kunzmann, M., Halverson, G. P., Scott, C., Minarik, W. G., and Wing, B. A. (2015). Geochemistry of Neoproterozoic black shales from Svalbard: Implications for oceanic redox conditions spanning Cryogenian glaciations. *Chem. Geol.* 417, 383–393. doi: 10.1016/j.chemgeo.2015.10.022

Lehmann, M. F., Bernasconi, S. M., Barbieri, A., and McKenzie, J. A. (2002). Preservation of organic matter and alteration of its carbon and nitrogen isotope composition during simulated and *in situ* early sedimentary diagenesis. *Geochim. Cosmochim. Acta* 66, 3573–3584. doi: 10.1016/S0016-7037(02)00968-7

Li, Z. X., Bogdanova, S., Collins, A. S., Davidson, A., De Waele, B., Ernst, R. E., et al. (2008). Assembly, configuration, and break-up history of Rodinia: a synthesis. *Precambrian Res.* 160, 179–210. doi: 10.1016/j.precamres.2007.04.021

Li, R. W., Chen, J., Zhang, S., Lei, J., Shen, Y., and Chen, X. (1999). Spatial and temporal variations in carbon and sulfur isotopic compositions of Sinian sedimentary rocks in the Yangtze platform, South China. *Precambrian Res.* 97, 59–75. doi: 10.1016/S0301-9268(99)00022-4

Li, C., Love, G. D., Lyons, T. W., Scott, C. T., Feng, L. J., Huang, J., et al. (2012). Evidence for a redox stratified Cryogenian marine basin, Datangpo Formation, South China. *Earth Planet. Sci. Lett.* 331, 246–256. doi: 10.1016/j.epsl.2012.03.018

Li, T. T., Zhu, G. Y., Zhao, K., and Chen, Z. Y. (2022). Geochemical characteristics of organic-rich intervals within the Cryogenian non-glacial Datangpo Formation in southeastern Yangtze Block-implications for paleoenvironment and its control on organic matter accumulation. *Precambrian Res.* 378, 106777. doi: 10.1016/j.precamres.2022.106777

Ma, Z. X., Liu, X. T., Yu, W. C., Du, Y. S., and Du, Q. D. (2019). Redox conditions and manganese metallogenesis in the Cryogenian Nanhua Basin: Insight from the basal Datangpo Formation of South China. *Palaeogeogr. Palaeoclimatol. Palaeoecol.* 529, 39–52. doi: 10.1016/j.palaeo.2019.05.031

Ma, X., Wang, J. S., Wang, Z., Algeo, T. J., Chen, C., Cen, Y., et al. (2023). Geochronological constraints on Cryogenian ice ages: Zircon U-Pb ages from a shelf section in South China. *Global Planet. Change* 222, 104071. doi: 10.1016/j.gloplacha.2023.104071

McKirdy, D. M., Burgess, J. M., Lemon, N. M., Yu, X. K., Cooper, A. M., Gostin, V. A., et al. (2001). A chemostratigraphic overview of the late Cryogenian interglacial sequence in the Adelaide Fold-Thrust Belt, South Australia. *Precambrian Res.* 106, 149–186. doi: 10.1016/S0301-9268(00)00130-3

Melezhik, V., Fallick, A. E., and Pokrovsky, B. G. (2005). Enigmatic nature of thick sedimentary carbonates depleted in ^{13}C beyond the canonical mantle value: the challenges to our understanding of the terrestrial carbon cycle. *Precambrian Res.* 137, 131–165. doi: 10.1016/j.precamres.2005.03.010

Meyer, K. M., Yu, M., Lehrmann, D., Van de Schootbrugge, B., and Payne, J. L. (2013). Constraints on Early Triassic carbon cycle dynamics from paired organic and inorganic carbon isotope records. *Earth Planet. Sci. Lett.* 361, 429–435. doi: 10.1016/j.epsl.2012.10.035

Möbius, J. (2013). Isotope fractionation during nitrogen remineralization (ammonification): Implications for nitrogen isotope biogeochemistry. *Geochim. Cosmochim. Acta* 105, 422–432. doi: 10.1016/j.gca.2012.11.048

Möbius, J., Lahajnar, N., and Emeis, K. C. (2010). Diagenetic control of nitrogen isotope ratios in Holocene sapropels and recent sediments from the Eastern Mediterranean Sea. *Biogeosciences* 7, 3901–3914. doi: 10.5194/bg-7-3901-2010

Moores, E. M. (1991). Southwest US-East Antarctic (SWEAT) connection: a hypothesis. *Geology* 19, 425–428. doi: 10.1130/0091-7613(1991)019<0425:SUSEAS>2.3.CO;2

Morgan, J. J. (2005). Kinetics of reaction between O_2 and Mn (II) species in aqueous solutions. *Geochim. Cosmochim. Acta* 69, 35–48. doi: 10.1016/j.gca.2004.06.013

Müller, P. J. (1977). C-N ratios in Pacific deep-sea sediments-effect of inorganic ammonium and organic nitrogen-compounds sorbed by clays. *Geochim. Cosmochim. Acta* 41, 765–776. doi: 10.1016/0016-7037(77)90047-3

Oehlert, A. M., and Swart, P. K. (2014). Interpreting carbonate and organic carbon isotope covariance in the sedimentary record. *Nat. Commun.* 5, 4673–4678. doi: 10.1038/ncomms5672

Olcott, A. N., Sessions, A. L., Corsetti, F. A., Kaufman, A. J., and De Oliviera, T. F. (2005). Biomarker evidence for photosynthesis during Neoproterozoic glaciation. *Science* 310, 471–474. doi: 10.1126/science.1115769

Pei, H. X., Fu, Y., Li, C., Li, Y. H., and An, Z. Z. (2017). Mineralization age and metallogenic environment of Daotuo manganese deposits in Guizhou: Evidence from Re-Os isotopes. *Chin. Sci. Bull.* 62, 3346–3355. doi: 10.1360/N972017-00450

Pei, H. X., Li, Y. H., Fu, Y., and Zhan, P. C. (2020). Metallogenic mechanism of "Datangpo Type" manganese deposits in Gaodi, Guizhou Province: constrains from sulfur and carbon isotopes. *Acta Geosci. Sin.* 41, 651–662. doi: 10.3975/cagsb.2020.070603

Peng, X., Zhu, X. K., Shi, F. Q., Yan, B., Zhang, F. F., Zhao, N. N., et al. (2019). A deep marine organic carbon reservoir in the non-glacial Cryogenian ocean (Nanhua Basin, South China) revealed by organic carbon isotopes. *Precambrian Res.* 321, 212–220. doi: 10.1016/j.precamres.2018.12.013

Pennock, J. R., Velinsky, D. J., Ludlam, J. M., Sharp, J. H., and Fogel, M. L. (1996). Isotopic fractionation of ammonium and nitrate during uptake by Skeletonema costatum: Implications for $\delta^{15}N$ dynamics under bloom conditions. *Limnol. Oceanogr.* 41, 451–459. doi: 10.4319/lo.1996.41.3.0451

Polgári, M., Hein, J. R., Tóth, A. L., Pál-Molnár, E., Vigh, T., Bíró, L., et al. (2012a). Microbial action formed Jurassic Mn-carbonate ore deposit in only a few hundred years (Úrkút, Hungary). *Geology* 40, 903–906. doi: 10.1130/G33304.1

Polgári, M., Hein, J. R., Vigh, T., Szabó-Drubina, M., Fórizs, I., Bíró, L., et al. (2012b). Microbial processes and the origin of the Úrkút manganese deposit, Hungary. *Ore Geol. Rev.* 47, 87–109. doi: 10.1016/j.oregeorev.2011.10.001

Qu, Y. Z., Xu, L. G., Mao, J. W., Pan, W., Zhan, P. C., and An, Z. Z. (2018). Carbon and oxygen isotope characteristics and mineralization of black shale-hosted manganese carbonate of Datangpo Formation in Tongren, Guizhou Province. *Miner. Deposits* 37, 50–66. doi: 10.16111/j.0258-7106.2018.01.004

Quan, T. M., Wright, J. D., and Falkowski, P. G. (2013). Co-variation of nitrogen isotopes and redox states through glacial-interglacial cycles in the Black Sea. *Geochim. Cosmochim. Acta* 112, 305–320. doi: 10.1016/j.gca.2013.02.029

Ray, J. S., Veizer, J., and Davis, W. J. (2003). C, O, Sr and Pb isotope systematics of carbonate sequences of the Vindhyan Supergroup, India: age, diagenesis, correlations and implications for global events. *Precambrian Res.* 121, 103–140. doi: 10.1016/S0301-9268(02)00223-1

Reis, A., Erhardt, A. M., McGlue, M. M., and Waite, L. (2019). Evaluating the effects of diagenesis on the $\delta^{13}C$ and $\delta^{18}O$ compositions of carbonates in a mud-rich depositional environment: A case study from the Midland Basin, USA. *Chem. Geol.* 524, 196–212. doi: 10.1016/j.chemgeo.2019.06.021

Riedman, L. A., Porter, S. M., Halverson, G. P., Hurtgen, M. T., and Junium, C. K. (2014). Organic-walled microfossil assemblages from glacial and interglacial Neoproterozoic units of Australia and Svalbard. *Geology* 42, 1011–1014. doi: 10.1130/G35901.1

Rieu, R., Allen, P. A., Plötze, M., and Pettke, T. (2007). Climatic cycles during a Neoproterozoic "snowball. *glacial epoch. Geology* 35, 299–302. doi: 10.1130/G23400A.1

Robinson, R. S., Kienast, M., Luiza Albuquerque, A., Altabet, M., Contreras, S., De Pol Holz, R., et al. (2012). A review of nitrogen isotopic alteration in marine sediments. *Paleoceanography* 27, PA4203. doi: 10.1029/2012PA002321

Rooney, A. D., Strauss, J. V., Brandon, A. D., and Macdonald, F. A. (2015). A Cryogenian chronology: Two long-lasting synchronous Neoproterozoic glaciations. *Geology* 43, 459–462. doi: 10.1130/G36511.1

Rooney, A. D., Yang, C., Condon, D. J., Zhu, M. Y., and Macdonald, F. A. (2020). U-Pb and Re-Os geochronology tracks stratigraphic condensation in the Sturtian snowball Earth aftermath. *Geology* 48, 625–629. doi: 10.1130/G47246.1

Roy, S. (2006). Sedimentary manganese metallogenesis in response to the evolution of the Earth system. *Earth-Sci. Rev.* 77, 273–305. doi: 10.1016/j.earscirev.2006.03.004

Roy, S., Bandopadhyay, P. C., Perseil, E. A., and Fukuoka, M. (1990). Late diagenetic changes in manganese ores of the Upper Proterozoic Penganga Group, India. *Ore Geol. Rev.* 5, 341–357. doi: 10.1016/0169-1368(90)90038-O

Scheller, E. L., Dickson, A. J., Canfield, D. E., Korte, C., Kristiansen, K. K., and Dahl, T. W. (2018). Ocean redox conditions between the snowballs-Geochemical constraints from Arena Formation, East Greenland. *Precambrian Res.* 319, 173–186. doi: 10.1016/j.precamres.2017.12.009

Shen, W. B., Zhu, X. K., Li, J., and Yan, B. (2022). Mechanism of organic matter accumulation in black shale of the Datangpo Formation: Insights from paleo-environmental variation during the Cryogenian non-glaciation. *Precambrian Res.* 383, 106889. doi: 10.1016/j.precamres.2022.106889

Sigman, D. M., Karsh, K. L., and Casciotti, K. L. (2009). Ocean process tracers: Nitrogen isotopes in the ocean. *Encyclopedia Ocean Sci.*, 40–54. doi: 10.1016/B978-0-12-409548-9.11605-7

Sperling, E. A., Carbone, C., Strauss, J. V., Johnston, D. T., Narbonne, G. M., and Macdonald, F. A. (2016). Oxygen, facies, and secular controls on the appearance of Cryogenian and Ediacaran body and trace fossils in the Mackenzie Mountains of northwestern Canada. *Geol. Soc Am. Bull.* 128, 558–575. doi: 10.1130/B31329.1

Stüeken, E. E., Kipp, M. A., Koehler, M. C., and Buick, R. (2016). The evolution of Earth's biogeochemical nitrogen cycle. *Earth-Sci. Rev.* 160, 220–239. doi: 10.1016/j.earscirev.2016.07.007

Swart, P. K. (2015). The geochemistry of carbonate diagenesis: The past, present and future. *Sedimentology* 62, 1233–1304. doi: 10.1111/sed.2015.62.issue-5

Swart, P. K., and Oehlert, A. M. (2018). Revised interpretations of stable C and O patterns in carbonate rocks resulting from meteoric diagenesis. *Sediment. Geol.* 364, 14–23. doi: 10.1016/j.sedgeo.2017.12.005

Tan, Z. Z., Jia, W. L., Li, J., Yin, L., Wang, S. S., Wu, J. X., et al. (2021). Geochemistry and molybdenum isotopes of the basal Datangpo Formation: Implications for ocean-redox conditions and organic matter accumulation during the Cryogenian interglaciation. *Palaeogeogr. Palaeoclimatol. Palaeoecol.* 563, 110169. doi: 10.1016/j.palaeo.2020.110169

Tebo, B. M., Bargar, J. R., Clement, B. G., Dick, G. J., Murray, K. J., Parker, D., et al. (2004). Biogenic manganese oxides: properties and mechanisms of formation. *Annu. Rev. Earth Planet. Sci.* 32, 287–328. doi: 10.1146/annurev.earth.32.101802.120213

Thomazo, C., Ader, M., and Philippot, P. (2011). Extreme ^{15}N-enrichments in 2.72-Gyr-old sediments: evidence for a turning point in the nitrogen cycle. *Geobiology* 9, 107–120. doi: 10.1111/j.1472-4669.2011.00271.x

Tribovillard, N., Algeo, T. J., Lyons, T., and Riboulleau, A. (2006). Trace metals as paleoredox and paleoproductivity proxies: an update. *Chem. Geol.* 232, 12–32. doi: 10.1016/j.chemgeo.2006.02.012

Tu, C. Y., Diamond, C. W., Stüeken, E. E., Cao, M. C., Pan, W., and Lyons, T. W. (2024). Dynamic evolution of marine productivity, redox, and biogeochemical cycling track local and global controls on Cryogenian sea-level change. *Geochim. Cosmochim. Acta* 365, 114–135. doi: 10.1016/j.gca.2023.12.005

Wang, P., Algeo, T. J., Zhou, Q., Yu, W. C., Du, Y. S., Qin, Y. J., et al. (2019b). Large accumulations of ^{34}S-enriched pyrite in a low-sulfate marine basin: The Sturtian Nanhua Basin, South China. *Precambrian Res.* 335, 105504. doi: 10.1016/j.precamres.2019.105504

Wang, P., Du, Y. S., Yu, W. C., Algeo, T. J., Zhou, Q., Xu, Y., et al. (2020). The chemical index of alteration (CIA) as a proxy for climate change during glacial-interglacial transitions in Earth history. *Earth-Sci. Rev.* 201, 103032. doi: 10.1016/j.earscirev.2019.103032

Wang, T. G., Li, M. J., Wang, C. J., Wang, G. L., Zhang, W. B., Shi, Q., et al. (2008). Organic molecular evidence in the Late Neoproterozoic Tillites for a palaeo-oceanic environment during the snowball Earth era in the Yangtze region, southern China. *Precambrian Res.* 162, 317–326. doi: 10.1016/j.precamres.2007.09.009

Wang, J., and Pan, G. T. (2009). Neoproterozoic South China palaeocontinents: an overview. *Acta Sediment. Sin.* 27, 818–825. doi: 10.14027/j.cnki.cjxb.2009.05.005

Wang, D., Zhu, X. K., Zhao, N. N., Yan, B., Li, X. H., Shi, F. Q., et al. (2019a). Timing of the termination of Sturtian glaciation: SIMS U-Pb zircon dating from South China. *J. Asian Earth Sci.* 177, 287–294. doi: 10.1016/j.jseaes.2019.03.015

Wei, W., Wang, D., Li, D., Ling, H. F., Chen, X., Wei, G. Y., et al. (2016). The marine redox change and nitrogen cycle in the Early Cryogenian interglacial time: Evidence from nitrogen isotopes and Mo contents of the basal Datangpo Formation, northeastern Guizhou, South China. *J. Earth Sci.* 27, 233–241. doi: 10.1007/s12583-015-0657-1

Wei, G. Y., Wei, W., Wang, D., Li, T., Yang, X. P., Shields, G. A., et al. (2020). Enhanced chemical weathering triggered an expansion of euxinic seawater in the aftermath of the Sturtian glaciation. *Earth Planet. Sci. Lett.* 539, 116244. doi: 10.1016/j.epsl.2020.116244

Wu, J. X., Tan, Z. Z., Jia, W. L., Chen, J., and Peng, P. A. (2024). Nitrogen isotopes and geochemistry of the basal Datangpo Formation: Contrasting redox conditions in the upper and lower water columns during the Cryogenian interglaciation period. *Palaeogeogr. Palaeoclimatol. Palaeoecol.* 637, 112005. doi: 10.1016/j.palaeo.2023.112005

Wu, C. Q., Zhang, Z. W., Xiao, J. F., Fu, Y. Z., Shao, S. X., Zheng, C. F., et al. (2016). Nanhuan manganese deposits within restricted basins of the southeastern Yangtze Platform, China: Constraints from geological and geochemical evidence. *Ore Geol. Rev.* 75, 76–99. doi: 10.1016/j.oregeorev.2015.12.003

Xiao, J. F., He, J. Y., Yang, H. Y., and Wu, C. Q. (2017). Comparison between Datangpo-type manganese ores and modern marine ferromanganese oxyhydroxide precipitates based on rare earth elements. *Ore Geol. Rev.* 89, 290–308. doi: 10.1016/j.oregeorev.2017.06.016

Yin, C. Y., Wang, Y. G., Tang, F., Wan, Y. S., Wang, Z. Q., Gao, L. Z., et al. (2006). SHRIMP II U-Pb zircon date from the Nanhuan Datangpo Formation in Songtao county, Guizhou province. *Acta Geol. Sin.* 80, 278–285.

Yonkee, W. A., Dehler, C. D., Link, P. K., Balgord, E. A., Keeley, J. A., Hayes, D. S., et al. (2014). Tectono-stratigraphic framework of Neoproterozoic to Cambrian strata, west-central US: Protracted rifting, glaciation, and evolution of the North American Cordilleran margin. *Earth-Sci. Rev.* 136, 59–95. doi: 10.1016/j.earscirev.2014.05.004

Yu, W. C., Algeo, T. J., Du, Y. S., Maynard, B., Guo, H., Zhou, Q., et al. (2016). Genesis of Cryogenian Datangpo manganese deposit: Hydrothermal influence and episodic post-glacial ventilation of Nanhua Basin, South China. *Palaeogeogr. Palaeoclimatol. Palaeoecol.* 459, 321–337. doi: 10.1016/j.palaeo.2016.05.023

Yu, W. C., Algeo, T. J., Du, Y. S., Zhou, Q., Wang, P., Xu, Y., et al. (2017). Newly discovered Sturtian cap carbonate in the Nanhua Basin, South China. *Precambrian Res.* 293, 112–130. doi: 10.1016/j.precamres.2017.03.011

Yu, W. C., Algeo, T. J., Zhou, Q., Du, Y. S., and Wang, P. (2020). Cryogenian cap carbonate models: A review and critical assessment. *Palaeogeogr. Palaeoclimatol. Palaeoecol.* 552, 109727. doi: 10.1016/j.palaeo.2020.109727

Yu, W. C., Polgári, M., Gyollai, I., Fintor, K., Szabó, M., Kovács, I., et al. (2019). Microbial metallogenesis of Cryogenian manganese ore deposits in South China. *Precambrian Res.* 322, 122–135. doi: 10.1016/j.precamres.2019.01.004

Zerkle, A. L., Junium, C. K., Canfield, D. E., and House, C. H. (2008). Production of ^{15}N-depleted biomass during cyanobacterial N_2-fixation at high Fe concentrations. *J. Geophys. Res.: Biogeo.* 113, G03014. doi: 10.1029/2007JG000651

Zhang, B., Cao, J., Hu, K., Liao, Z. W., Zhang, R., Zhang, Y., et al. (2024a). A new negative carbon isotope interval caused by manganese redox cycling after the Shuram excursion. *J. Geophys. Res.-Solid Earth* 129, e2023JB028307. doi: 10.1029/2023JB028307

Zhang, Y., Liao, Z. W., Cao, J., Lash, G. G., Wei, Y., Shi, Q., et al. (2024b). Climate variability during the late Ediacaran: Insights from episodic deposition of black shale-hosted Mn−carbonates in South China. *Chem. Geol.* 646, 121910. doi: 10.1016/j.chemgeo.2023.121910

Zhao, K., Lang, X. G., Zhu, G. Y., Feng, M. S., He, R., Guan, C. G., et al. (2022). Low marine sulfate levels during the initiation of the Cryogenian Marinoan glaciation. *Precambrian Res.* 377, 106737. doi: 10.1016/j.precamres.2022.106737

Zhou, Q., Du, Y. S., and Qin, Y. (2013). Ancient natural gas seepage sedimentary-type manganese metallogenic system and ore-forming model: a case study of Datangpo type manganese deposits formed in rift basin of Nanhua period along Guizhou-Hunan-Chongqing border area. *Miner. Deposits* 32, 457–466. doi: 10.16111/j.0258-7106.2013.03.001

Zhou, Q., Du, Y. S., Yan, J. X., Zhang, M. Q., and Yin, S. L. (2007). Geological and geochemical characteristics of the cold seep carbonates in the early nanhua system in datangpo, songtao, Guizhou Province. *Earth Sci.* 32, 845–852.

Zhou, Q., Du, Y. S., Yuan, L. J., Zhang, S., Yu, W. C., Yang, S. T., et al. (2016). The Structure of the Wuling Rift Basin and its control on the manganese deposit during the Nanhua period in Guizhou-Hunan-Chongqing border area, South China. *Earth Sci.* 41, 177–188. doi: 10.3799/dqkx.2016.014

Zhou, C. M., Huyskens, M. H., Lang, X. G., Xiao, S. H., and Yin, Q. Z. (2019). Calibrating the terminations of Cryogenian global glaciations. *Geology* 47, 251–254. doi: 10.1130/G45719.1

Zhou, C. M., Huyskens, M. H., Xiao, S. H., and Yin, Q. Z. (2020). Refining the termination age of the Cryogenian Sturtian glaciation in South China. *Palaeoworld* 29, 462–468. doi: 10.1016/j.palwor.2020.04.002

Zhou, C., Tucker, R., Xiao, S. H., Peng, Z. X., Yuan, X. L., and Chen, Z. (2004). New constraints on the ages of Neoproterozoic glaciations in south China. *Geology* 32, 437–440. doi: 10.1130/G20286.1

Zhou, Q., Wu, C. L., Hu, X. Y., Yang, B. N., Zhang, X. L., Du, Y. S., et al. (2022). A new metallogenic model for the giant manganese deposits in northeastern Guizhou, China. *Ore Geol. Rev.* 149, 105070. doi: 10.1016/j.oregeorev.2022.105070

Zhu, G. Y., Li, T. T., Zhang, Z. Y., Zhao, K., Song, H. Y., Wang, P. J., et al. (2022). Nitrogen isotope evidence for oxygenated upper ocean during the Cryogenian interglacial period. *Chem. Geol.* 604, 120929. doi: 10.1016/j.chemgeo.2022.120929

Zhu, G. Y., Li, T. T., Zhao, K., Zhang, Z. Y., Chen, W. Y., Yan, H. H., et al. (2019). Excellent source rocks discovered in the Cryogenian interglacial deposits in South China: Geology, geochemistry, and hydrocarbon potential. *Precambrian Res.* 333, 105455. doi: 10.1016/j.precamres.2019.105455